

Review

A Review of State Estimation Techniques for Grid-Connected PMSG-Based Wind Turbine Systems

Ganesh Mayilsamy ¹, Kumarasamy Palanimuthu ¹, Raghul Venkateswaran ¹,
Ruban Periyannayagam Antonyamsamy ¹, Seong Ryong Lee ¹, Dongran Song ² and Young Hoon Joo ^{1,*}

¹ School of IT Information and Control Engineering, Kunsan National University, 588 Daehak-ro, Gunsan-si 54150, Republic of Korea; ganeshm.vjm@gmail.com (G.M.); kumaras001@gmail.com (K.P.); raghulsmart008@gmail.com (R.V.); arubanpnr@gmail.com (R.P.A.); srlee@kunsan.ac.kr (S.R.L.)

² School of Automation, Central South University, Changsha 410083, China; humble_szy@163.com

* Correspondence: yhjoo@kunsan.ac.kr

Abstract: The power system network grows yearly with a large number of nonlinear power generation systems. In this scenario, accurate modeling, control, and monitoring of interface systems and energy conversion systems are critical to the reliability and performance of the overall power system. In this trend, the permanent magnet synchronous generator (PMSG)-based wind turbine systems (WTS) equipped with a full-rated converter significantly contribute to the development of new and renewable energy generation. The various components and control systems involved in operating these systems introduce higher complexity, uncertainty, and highly nonlinear control challenges. To deal with this, state estimation remains an ideal and reliable procedure in the relevant control of the entire WTS. In essence, state estimation can be useful in control procedures, such as low-voltage ride-through operation, active power regulation, stator fault diagnosis, maximum power point tracking, and sensor faults, as it reduces the effects of noise and reveals all hidden variables. However, many advanced studies on state estimation of PMSG-based WTS deal with real-time information of operating variables through filters and observers, analysis, and summary of these strategies are still lacking. Therefore, this article aims to present a review of state-of-the-art estimation methods that facilitate advances in wind energy technology, recent power generation trends, and challenges in nonlinear modeling. This review article enables readers to understand the current trends in state estimation methods and related issues of designing control, filtering, and state observers. Finally, the conclusion of the review demonstrates the direction of future research.

Keywords: wind turbine system; permanent magnet synchronous generator; variable speed wind turbine; state estimation technique; Kalman filter



Citation: Mayilsamy, G.; Palanimuthu, K.; Venkateswaran, R.; Antonyamsamy, R.P.; Lee, S.R.; Song, D.; Joo, Y.H. A Review of State Estimation Techniques for Grid-Connected PMSG-Based Wind Turbine Systems. *Energies* **2023**, *16*, 634. <https://doi.org/10.3390/en16020634>

Academic Editor: Francesco Castellani

Received: 27 November 2022

Revised: 24 December 2022

Accepted: 4 January 2023

Published: 5 January 2023



Copyright: © 2023 by the authors. Licensee MDPI, Basel, Switzerland. This article is an open access article distributed under the terms and conditions of the Creative Commons Attribution (CC BY) license (<https://creativecommons.org/licenses/by/4.0/>).

1. Introduction

The past few decades have seen significant advances in research and investigation into the technologies that make wind energy more feasible, and the methods to improve such technologies are getting explored by researchers. The significance of grid-connected wind turbine systems (WTS) on power networks is becoming more evident as the production and deployment of renewable energy sources expand [1–4]. In 2021, the worldwide wind power installed capacity has increased by 12.4%, reaching 837 GW, an increase of 93.6 GW from the previous peak in 2020 [5]. It is expected that in the future, variable-speed WTSs will be the best choice to increase power production in onshore/offshore WTS and contribute to green energy contributions [6,7].

Large offshore wind turbines offer the best return on investment when equipped with a compact and lightweight generator and drive train. This is because the reduction in the volume of the nacelle also reduces the mass of the tower and foundation or floating platform and the cost of these components [8]. Interestingly, direct-drive (DD)

synchronous generator (SG)-based wind turbine systems are receiving considerable attention worldwide due to the increasing electricity demand [9–12]. Several designs in DD generators have recently been introduced, such as transverse flux-permanent magnets and magnetic vernier machines [13–16]. Among them, one of the most suitable alternatives to the permanent magnet SG (PMSG) is the permanent magnet vernier generator (PMVG), developed with improvement in parameters, such as high torque density, low torque ripple, and lower weight [17,18]. In addition, the authors of [19] have experimentally verified the superior control performance of PMVG over the PMSG for wind turbine (WT) applications. The recent green power systems have started to include sophisticated area monitoring and control systems for wind power in response to the rapid expansion of WTS. Recently, various control strategies have been proposed to improve stable power production and the performance of PMVG-based WTS [20–22].

Most wind turbine applications assume the system parameters to be constant regardless of operating conditions. However, if the accuracy of this assumption needs to be verified or if the user has reason to believe that the manufacturer-supplied control parameters are inaccurate or outdated, model verification is necessary to receive values that consider the definite operating point [23,24]. For example, this need has been recognized in the United States, where the North American Electrical Reliability Corporation (NERC) has published reliability guidelines regarding generator model specification validation for generators [25] exceeding specific power ratings. These specifications include synchronous machines and other inverter-based generators. NERC proposes two methods for validating and calibrating generator models. (1) Take the generating machine out of the operation and perform specific tests. (2) Measuring systems similar to disturbance measures, such as Phasor Measurement Units (PMUs), data loggers, and error recorders. Dynamic state estimators get actual information from system states to make a reliable control structure that can adapt to the intrinsic intermittency of wind energy generation.

Generally, sensor redundancy can be ensured in two ways: state observers or state estimators. Monitoring sensors and other equipment generating residuals used for fault diagnosis rely heavily on this redundancy [26,27]. The growing power system network has instigated many control challenges to interface the generating units to the power system network. To deal with the adaptation challenges of the generating units with the power system network, complete knowledge about the behavioral model of the generating units is of prime importance [28,29]. Moreover, real-time state estimation is essential for control systems for stable wind power system operation.

On the other hand, in the literature, dynamic state estimation approaches can be extensively divided into two categories. The most common approach, known as Kalman Filtering (KF), goes into the first category [30]. Extended Kalman Filter (EKF) [31], Unscented Kalman Filter (UKF) [32], and Cubature Kalman Filter (CKF) [33] are a few examples of techniques that fall into this category. Due to the inherent nonlinear nature of power systems, EKF is a good candidate for state estimation [34], which linearizes the nonlinear functions by retaining the first-order components of the Taylor series expansion [35]. Particle filtering (PF) represents the second category of methods [36]. It will attain high estimate precision under Gaussian and non-Gaussian noise with considerable computational complexity [37,38]. Decentralized methods have been offered alongside centralized ones. Distributed Particle Filter (DPF) is superior to centralized algorithms in terms of tracking accuracy and resilience in a dynamic setting [39,40]. With these discussions, KF-based approaches are predominantly prevalent in state estimation-based control methods of PMSG-based wind power applications.

The Kalman Filter further forecasts the system state by utilizing the estimates from the past. One method to guarantee sensor redundancy is to use state estimators. This redundancy is essential for monitoring the many systems and sensors used in PMSG-based WTSs and creating residuals that could later be applied to fault diagnosis. Software sensors make excellent use of state observers and estimators. The latter considers the process' statistical features, their primary distinction. The covariance matrices of system states,

the noise in the process, and the measurement are used by state estimators. Additionally, they can learn how to operate uncertainties or the effects impact of faults in the system. Moreover, they might be less sensitive to noise. Moreover, the linear Kalman filtering-based methods are analyzed in [26,41,42], in which the [42] accounts for the issues of sensor fusion and error correction. Further, EKF-based methods are analyzed in [43–45], and the UKF-based methods are discussed in [46–48]. Then the adaptive filtering and Particle filter-based methods are analyzed in [49,50]. Additionally, a non-standard EKF is proposed for wind-speed estimations in [51]. In the context of electrical grid reliability, the voltage ride-through (VRT) capability of a WTS is of due importance to comply with the requirement of grid code. The grid code usually fixes certain constraints to the operations of WTS under fault conditions in the electrical grid [52]. The usage of a fully rated power converter in PMSG-based WTS provides enough flexibility to supply a greater amount of reactive power support to the electric grid in the time of such fault occurrence. There have been numerous studies found in this area to achieve better performance of LVRT with PMSG-based WTS. Out of which, the mode shift control-based LVRT [53], an ANFIS-based LVRT approach [54], and the coordinated active and reactive power control strategy [55] are the few recent works worth mentioning. The measured dc-link voltage has been used in all these methods to determine how well the WTS's LVRT will operate. Therefore, if there is any noise in the measured dc-link voltage or if the dc-link voltage measurement device is not working properly, the approach may have problems. Such a discrepancy is effectively addressed through state estimation techniques in [56]. In addition, the IoT-enabled state estimation methods are proposed to monitor and measure the performance of the PMSG-based WTS [42]. In this respect, many state estimation methods target the grid-connected PMSG-based WTS for reliable power production. Thus, the summary of the contribution is given as follows:

1. A mathematical model of the nonlinear PMSG-based WTS is presented, including the dynamics of the drive train, machine side converter (MSC) control, dc-link voltage control, and grid side converter (GSC) control.
2. Principles of state estimation techniques with classical KF, EKF, AEKF, ENKF, UKF, CKF, and ACKF are reviewed with their merits and limitations.
3. The application of state estimation techniques for WTS control, fault diagnosis, LVRT operation, and observers for sensorless control of WTS is highlighted.
4. State estimation techniques employed in pitch and yaw control of WTSs are discussed.

The article is structured as follows. Section 2 highlights the modeling of PMSG-based WTS structures. The discussion on state estimation procedures of the linearized model of PMSG-based WTS is given in Section 3. State estimation with nonlinear modeling of PMSG-based WTSs are discussed in Section 4. A review of the state estimation techniques for PMSG-based WTS fault diagnosis is given in Section 5. Section 6 discusses the observers and sensorless control of PMSG-based WTS. Section 7 deals with the application of state estimation techniques in pitch and yaw control of WTSs. Finally, the review article is concluded in Section 8.

2. Modeling of PMSG-Based WTS Structures

The overall structure of the WTS is depicted in Figure 1; the kinetic energy of atmospheric wind can be captured by the rotating blades of the horizontal axes wind turbine. The rotating blades are attached to the turbine shaft and coupled with the multi-pole three-phase PMSG machine. In general, most of the commercial PMSG-based WTSs are interfaced with the electric utility grid through the fully rated three-phase back-to-back power converters. Based on the power rating of the system, the converter may have different configurations from two-level to multi-level. The MSC is usually configured to control the operating speed of PMSG to its optimum value with the objective of extracting maximum wind power, during which the GSC establishes a dc-link voltage regulation. The dc-link acts as the buffer between the GSC and MSC, any power difference between the converters causes dc-link voltage fluctuations. Then, the GSC regulates the dc-link

voltage by adjusting the active power component of grid side dq -axes current. Moreover, the dq -axes currents of both converters are achieved by vector control theory. Further, it provides the decoupled nature of control between the MSC and GSC [57]. Thus the overall structure of PMSG-based WTS can be modeled as the following different systems: mechanical characteristics of the wind turbine system, PMSG modeling, dc-link, and modeling of grid system [58].

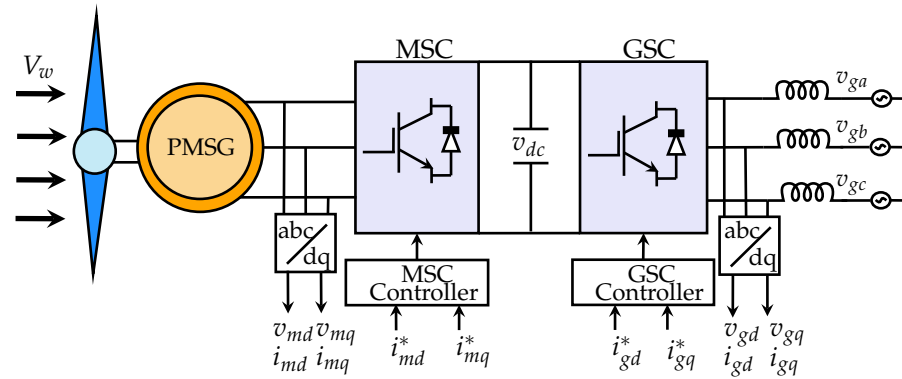


Figure 1. Schematic representation of PMSG-based WTS.

2.1. Mechanical Characteristics of Wind Turbine Systems

The aerodynamic power extracted by the rotating turbine blade can be quantified by the following mathematical model [19,59]:

$$P = \frac{1}{2} \rho A V_w^3 C_p(\lambda, \beta), \tag{1}$$

where ρ gives the density of air, V_w denotes the wind velocity, and $A = \pi R^2$ is the area covered by the rotating blades. Here, R stands for the radius of the blade. λ is the tip speed ratio (TSR) defined as [60,61]:

$$\lambda = \frac{\omega_m R}{V}. \tag{2}$$

where ω_m is the rotor speed of the turbine. The exponential approximation of WT power coefficient $C_p(\lambda, \beta)$ is defined as [58]:

$$C_p(\lambda, \beta) = 0.5176 \left(\frac{116}{\lambda_i} - 0.4\beta - 5 \right) \exp\left(\frac{-21}{\lambda_i}\right) + 0.0068\lambda \tag{3}$$

where

$$\frac{1}{\lambda_i} = \frac{1}{\lambda + 0.08\beta} - \frac{0.035}{\beta^3 + 1}$$

Next, the model of the drive train can be formulated by utilizing the single-mass model as follows [62,63]:

$$\frac{d\omega_m}{dt} = \frac{1}{J_{eq}} (T_{ad} - T_{em} - B\omega_m) \tag{4}$$

where T_{ad} is the aerodynamic torque of the turbine shaft, J_{eq} is the net inertia of the rotating shaft, B is the viscous friction coefficient, and T_{em} denotes the electromagnetic torque of the PMSG machine.

2.2. Modeling of Generator, dc-Link, and Grid

The PMSG is generally modeled in the $d - q$ equivalent circuit as follows [64]:

$$\begin{cases} v_{md} = R_s i_{md} + L_{md} \frac{di_{md}}{dt} - \omega_e L_{mq} i_{mq} \\ v_{mq} = R_s i_{mq} + L_{mq} \frac{di_{mq}}{dt} + \omega_e L_{md} i_{md} + \omega_e \Psi_f \end{cases} \quad (5)$$

where R_s denotes the resistance of the stator winding in Ω , v_{md} , v_{mq} , i_{md} , and i_{mq} are the dq -axes stator voltages and currents, L_{md} and L_{mq} are the inductances of stator winding, Ψ_f denotes the airgap flux, and ω_e is the angular frequency of stator voltages, which is equal to $P \times \omega_m$. In which P denotes the number of PMSG stator pole pairs.

Then the electromagnetic torque in the PMSG is written as

$$T_e = 1.5P\Psi_f i_{mq} \quad (6)$$

Further, an electrical dc-link acts as an interlink between the electrical grid and PMSG to transfer the power. Hence, the dc-link can be expressed by [22,65]

$$Cv_{dc} \frac{dv_{dc}}{dt} = P_e - P_g \quad (7)$$

where v_{dc} denotes the dc-link voltage in V , C is the dc-link capacitance, P_e gives the quantification of power flowing to the dc-link, and P_g is the power passing to the electrical grid.

The electricity grid is interfaced to the dc-link through the GSC via a RL filter, the dynamics of the filter can also be expressed in a dq frame [20,21]:

$$\begin{cases} v_{df} = R_f i_{gd} + L_{gd} \frac{di_{gd}}{dt} - \omega_f L_f i_{gq} + v_{gd} \\ v_{qf} = R_f i_{gq} + L_{gq} \frac{di_{gq}}{dt} + \omega_f L_f i_{gd} + v_{gq} \end{cases} \quad (8)$$

where ω_f denotes the angular frequency of the grid voltage, L_f and R_f are the inductance and resistance of the RL filter, v_{gd} , v_{gq} , v_{df} , and v_{qf} are the d and q -axis voltages of the grid and converter side, respectively, and i_{gd} and i_{gq} are the d and q -axis filter currents.

Then, the active and reactive power transfer to the grid can be expressed by

$$\begin{cases} P_g = 1.5(v_{gd} i_{gd} + v_{gq} i_{gq}) \\ Q_g = 1.5(v_{gq} i_{gd} - v_{gd} i_{gq}) \end{cases} \quad (9)$$

The mathematical expressions from (1) to (9) describe the model of different components of WTS. From those models, it can be inferred that the parameters such as MSC dq -axes currents and GSC dq -axes currents need to be controlled to achieve the power transfer task in the expected way. Moreover, the objective of such control is to get the rotor speed ω_m and dc-link voltage v_{dc} to the reference values. To achieve this control task, the parameters are required to be the known value in the control loop. In this regard, many sensors, such as speed sensor, current sensors, and voltage sensor, are used to measure the signals. Due to many factors, such as unknown interference, aging, calibration errors, and approximation errors, there may be some noises introduced in the measured signals. This unknown noise signal will have severe effects on the control performance. Hence to overcome this issue, state estimation techniques are found to be an ideal choice to estimate the parameters required to be used in control systems.

3. State Estimation with Linearized Model of PMSG-Based WTSs

The majority of contemporary WTSs features many sensors that, using a sequence of readings, estimate hidden (unknown) states. Providing an accurate and precise estimation of the hidden states in the presence of uncertainty is one of the main issues faced in the control of WTSs. One of the most remarkable and widespread estimate algorithms for the linear system is the Kalman filter. It is a significant mathematical tool used in the stochastic

estimation of sensor measurement noises. It was introduced by Rudolph E. Kalman in the year 1960 by describing a recursive solution to discrete data linear filtering. Moreover, the Kalman filter is a set of mathematical expressions to implement a predictor-corrector type estimator that is optimal in the view that it minimizes the estimated error covariance provided when some constraints are met. There have been a variety of research that deals with the application of the Kalman filter in the area of navigation and autonomous decision making. The Kalman filter generates hidden variable estimates based on unreliable and uncertain measurements. The Kalman filter additionally forecasts the system state based on estimates from the past [66].

Moreover, the dynamic model of PMSG given in (5) can be resolved into a product of states and input. The dq -axes current can be taken as the states, with input parameters of dq -axes voltage and angular speed ω_m . The dynamics of such a state space model of PMSG exhibit a nonlinear nature because it has the product of states and the input. The following dynamics of states can be obtained from (5)

$$\begin{cases} \dot{i}_{md} = \frac{v_{md} - R_s i_{md} + \omega_e L_{mq} i_{mq}}{L_{md}} \\ \dot{i}_{mq} = \frac{v_{mq} - R_s i_{mq} - \omega_e L_{md} i_{md} - \omega_e \Psi_f}{L_{mq}} \end{cases} \quad (10)$$

The real-time behavior of control algorithms implemented in digital signal processors is studied through the discretization of the model. Hence, (10) is required to be discretized. However, in practice, the discretization of the nonlinear model is very tedious. Therefore, the Taylor series expansion is most widely utilized to obtain a linear model as follows:

$$\begin{bmatrix} i_{md_{k+1}} \\ i_{mq_{k+1}} \end{bmatrix} = F_k \begin{bmatrix} i_{md_k} \\ i_{mq_k} \end{bmatrix} + G_k \begin{bmatrix} v_{md_k} \\ v_{mq_k} \end{bmatrix} + H_k \quad (11)$$

where

$$F_k = \begin{bmatrix} 1 - R_s/L_{md} & T_s P \omega_{m_k} \\ -T_s P \omega_{m_k} & 1 - R_s T_s/L_{mq} \end{bmatrix}; G_k = \begin{bmatrix} T_s/L_{md} & 0 \\ 0 & T_s/L_{mq} \end{bmatrix}; \text{ and } H_k = \begin{bmatrix} 0 \\ T_s P \omega_{m_k} \Psi_f/L_{mq} \end{bmatrix}$$

and T_s is the sampling period.

The above linear model may introduce significant errors in the parameters of the system. The Kalman filter for the estimation of states of the PMSG can be explained as follows:

$$\begin{cases} \hat{x}_{k+1} = A_k \hat{x}_k + B_k u_k \\ \hat{y}_k = C \hat{x}_k \end{cases} \quad (12)$$

where $x \in$ the states of process, $u \in$ the input variables, and $y \in$ the output variables of the process. A , B , and C are, respectively, the state, input, and output matrices. n_x , n_u , and n_y are the number of states, inputs, and measurements, respectively. k denotes the sampling time.

The linear model of the PMSG dq -axis currents in (11) can be modified to the form specified in (12) by combining the G and H matrices with the input vector being modified for three elements, as given below.

$$\begin{bmatrix} i_{md_{k+1}} \\ i_{mq_{k+1}} \end{bmatrix} = A_k \begin{bmatrix} i_{md_k} \\ i_{mq_k} \end{bmatrix} + B_k \begin{bmatrix} v_{md_k} \\ v_{mq_k} \\ \Psi_f \end{bmatrix} \quad (13)$$

where

$$A_k = F_k; B_k = \begin{bmatrix} T_s/L_{md} & 0 & 0 \\ 0 & T_s/L_{mq} & -T_s P \omega_{m_k}/L_{mq} \end{bmatrix}; \text{ and } C = \begin{bmatrix} 1 & 0 \\ 0 & 1 \end{bmatrix}.$$

Then, the classical Kalman filtering algorithm for the prediction and updating of the states can be formulated as follows;

Prediction phase:

$$\hat{P}_k = A_k P_k^* A_k^T + Q_k \quad (14)$$

Update phase:

$$\begin{cases} K_k = \hat{P}_k C^T (C \hat{P}_k C^T + R_k)^{-1} \\ \hat{x}_{k+1}^* = \hat{x}_k + K_k (y_k - C \hat{x}_k) \\ \hat{P}_k^* = (I - K_k C) \hat{P}_k \end{cases} \quad (15)$$

where, P is the state covariance matrix, and Q and R are the process and measurement noises covariance matrices. K and y are the Kalman gain and measurements from the process, respectively, and the superscript $*$ indicates the corrected estimation.

The above process of estimating the dq -axes currents can be adapted to the grid-side parameters with a suitable model. Further, any of the required operating parameters for the control of WTSs, such as pitch angle β of yaw angle Θ_{yaw} , can be modeled in state space, and the Kalman filtering can be applied for the estimation.

The main advantage of the Kalman filter is its ability to provide the quality of the estimate and its relatively low complexity. However, its main shortcoming is that it provides accurate results only for Gaussian and linear models.

4. State Estimation with Nonlinear Modeling of PMSG-Based WTSs

4.1. Extended Kalman Filter-Based Dynamic State Estimation

The extended Kalman filter is the nonlinear extension of the classical Kalman filter, which introduces the Taylor series expansion of state function for linearization. The estimation of the state covariance matrix is calculated using this linearization. However, because only the present estimated state is employed in this linearization, the introduced error is supposed to be smaller.

The generalized nonlinear model for EKF can be formulated as

$$\begin{cases} \hat{x}_{k+1} = f \hat{x}_k + u_k \\ y_k = h \hat{x}_k \end{cases} \quad (16)$$

where f and h are the state and measurement functions, respectively. Then, by utilizing (11), the EKF algorithm can be formulated as follows [67]:

Prediction phase:

$$\hat{P}_k = F_k \hat{P}_{k-1} F_k^T + Q_k \quad (17)$$

Update phase:

$$\begin{cases} K_k = \hat{P}_k H_k^T (H_k \hat{P}_k H_k^T + R_k)^{-1} \\ \hat{x}_k^* = \hat{x}_k + K_k (y_k - \hat{y}_k) \\ \hat{P}_k^* = (I - K_k H_k) \hat{P}_k \end{cases} \quad (18)$$

where F is the Jacobians of the state functions, and H is the Jacobians of the measurement functions.

The generalized models (5)–(9) of various systems of a PMSG-based WTS are widely applied in the analysis and control of WTS. In addition to this, the authors in [45,56] have utilized a detailed model of WTS, including the behavior of controllers. Specifically, unlike the traditional approach of dc-link regulation through the GSC, they have utilized the grid-side MPPT control approach. Hence by the principle of grid-side MPPT control,

the dc-link voltage is regulated by the q -axis control loop of MSC, and the d -axis can be used to inject the reactive power into the generator. The authors of [45] have addressed the nonlinear issue of anti-windup loops in the current loop's proportional-integral-derivative (PID) controllers, which have not been considered in many PMSG modeling. In addition, to the state variables given in (1) to (8), the authors [45,56] have considered some additional intermediate state variables $M_1, M_2, M_3, M_4, M_5, M_6, M_7,$ and M_8 . The intermediate state variables are derived from the integral of the error signal from dq -axes of MSC and GSC current control loops (for better understanding, the readers are referred to [45] for detailed information). Then, a modified drive train model is introduced with three state variables by considering the two mass drive train models and the stiffness of the rotating shaft. With the two mass drive train models, the generator speed ω_m , wind turbine speed ω_t , and the shaft twist angle α in radians are taken as the state variables of the drive train. Finally, a complete nonlinear state space model is formed with 16 state variables. Following that, EKF is suggested for the system's state estimation due to the model's nonlinearity, and all state space equations are modified for EKF implementation. The state estimator functions as a filter to receive some unprocessed observations from the system and estimates each variable using state space equations. The EKF estimation model utilizes the information of measurements such as grid and machine voltages/currents, dc-link voltage, and rotor speed.

The presented EKF state estimation model of the system is verified for robustness and efficiency through a system simulation of a 2.5 MW grid-connected wind turbine system, as depicted in Figures 2 and 3. The test procedure assumes four different cases of study for state estimation; a system with normal operation is taken as case-i, case-ii considers state estimation with measurement noise, case-iii is taken with fluctuating wind velocity, and case-iv is considered with a short circuit fault near the PMSG. The authors have made an extensive comparative analysis of the estimated parameters with the values of simulated parameters and the 11-variable state model presented in [68]. The authors have justified that their EKF state estimation method is of better accuracy. Hence the possible application of the presented state estimation technique with 16 variable state models can be extended to the nonlinear control of PMSG-based WTS during transients and disturbances.

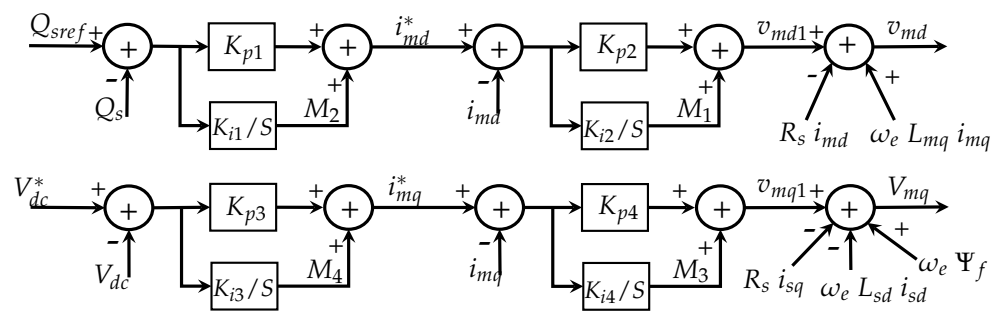


Figure 2. MSC control scheme for dc-link voltage regulation.

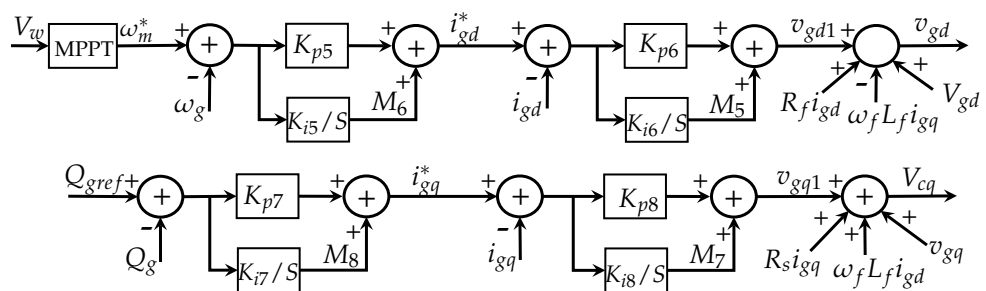


Figure 3. GSC control scheme with MPPT control and reactive power injection for LVRT applications.

Further, the article in [56] extends the application of the EKF state estimation technique to enhance the LVRT capability of the PMSG-based WTS. The state estimation algorithm

facilitates the removal of the dc-link voltage measuring system and generator speed measurement. In addition to this, the measurement system noise is also minimized. Then the applicability of the presented EKF-based state estimation technique for LVRT compatibility is verified by different case studies. The “EON” grid code given in [69] is extensively used in the case studies with the following fault types in the grid:

1. A severe three-phase to ground fault at the PMSG bus with a fault duration of 150 ms is considered case-i.
2. The case-i fault is taken in addition to a dc-link measurement noise as case-ii fault. The measurement noise model is expressed as $v_{dc(measured)} = v_{dc(actual)} + 0.0066 \times rand$.
3. A three-phase to ground fault, which causes the grid voltage to drop 0.15 pu for a longer duration of 625 ms, is assumed as a case-iii.
4. The case-iii fault is taken in addition to a dc-link measurement noise as case-iv fault.

Finally, the authors of [56] have substantiated the EKF-base state estimation technique by demonstrating the enhanced performance in LVRT compatibility of PMSG-based WTS. Since the input signals are estimated, the system performance is immune to noise in measurements. Further, the scheme solely relies on estimated values of v_{dc} and ω_m ; it is claimed to be robust against the failure of the dc-link and generator speed sensing system. The method has a drawback of poor voltage regulation due to the fact that the MSC input voltage varies with the rotor speed, whereas the grid voltage is constant.

4.2. Adaptive Extended Kalman Filter-Based Dynamic State Estimation

On the other hand, the erroneous noise statistical features may result in significant inaccuracies because the typical EKF requires accurate knowledge of the prior statistical behavior of noise. To deal with this issue, the authors of [70] suggest a dynamic analogous technique for the wind farm network with PMSG using the adaptive extended Kalman filters (AEKF) to decrease the dimension of the system model and enhance simulation efficacy while maintaining accuracy. In this article, the extended state variables are combined with the dynamic model of the generator, the equivalent parameters of WTS that need to be recognized are included, and an online variable identification approach based on EKF theory is proposed. Then, the adaptive system is implemented into EKF to approximate the process and measurement of noise covariance in real-time through the Sage–Husa estimator, eliminating the impact of random noise on the precision of estimation.

Concisely, the contribution of [70] can be summarized as the EKF estimation of wind farm equivalence to outperform the optimization technologies in terms of convergence and calculation complexity. Moreover, the EKF uses adaptive technology to estimate the process and measurement noise covariance in real-time using the Sage–Husa estimator, removing the effect of random noise. The AEKF technique-based state estimation is validated with an equivalent model containing one machine as an example; the methodology and findings are also suitable to the one-machine equivalence of a network of WTs in the multi-system network.

The functional flowchart of AEKF-based parameter estimation for the PMSG-based WTS is given in Figure 4. The method involves the selection of initial state variables x_0 , extended state variables x' , and deterministic state variables u_0 , the details of which are given below:

$$\begin{cases} x_0 = [i_{md}, i_{mq}, i_{\omega_m}, v_{dc}, i_{gd}, i_{gq}] \\ x' = [L_f, L_{md}, L_{mq}, \Psi_f, C] \\ u_0 = [v_{gd_{eq}}, v_{gq_{eq}}, v_{df_{eq}}, v_{qf_{eq}}, v_{md_{eq}}, v_{mq_{eq}}] \end{cases} \quad (19)$$

where u_0 comprises the equivalent dq -axes voltages of the grid, machine, and ac-side of the filter. The authors have considered a wind farm with M number of WT, each of which has a PMSG of different capacity S . The procedure to approximate the equivalent dq -axes voltages can be referred from [70].

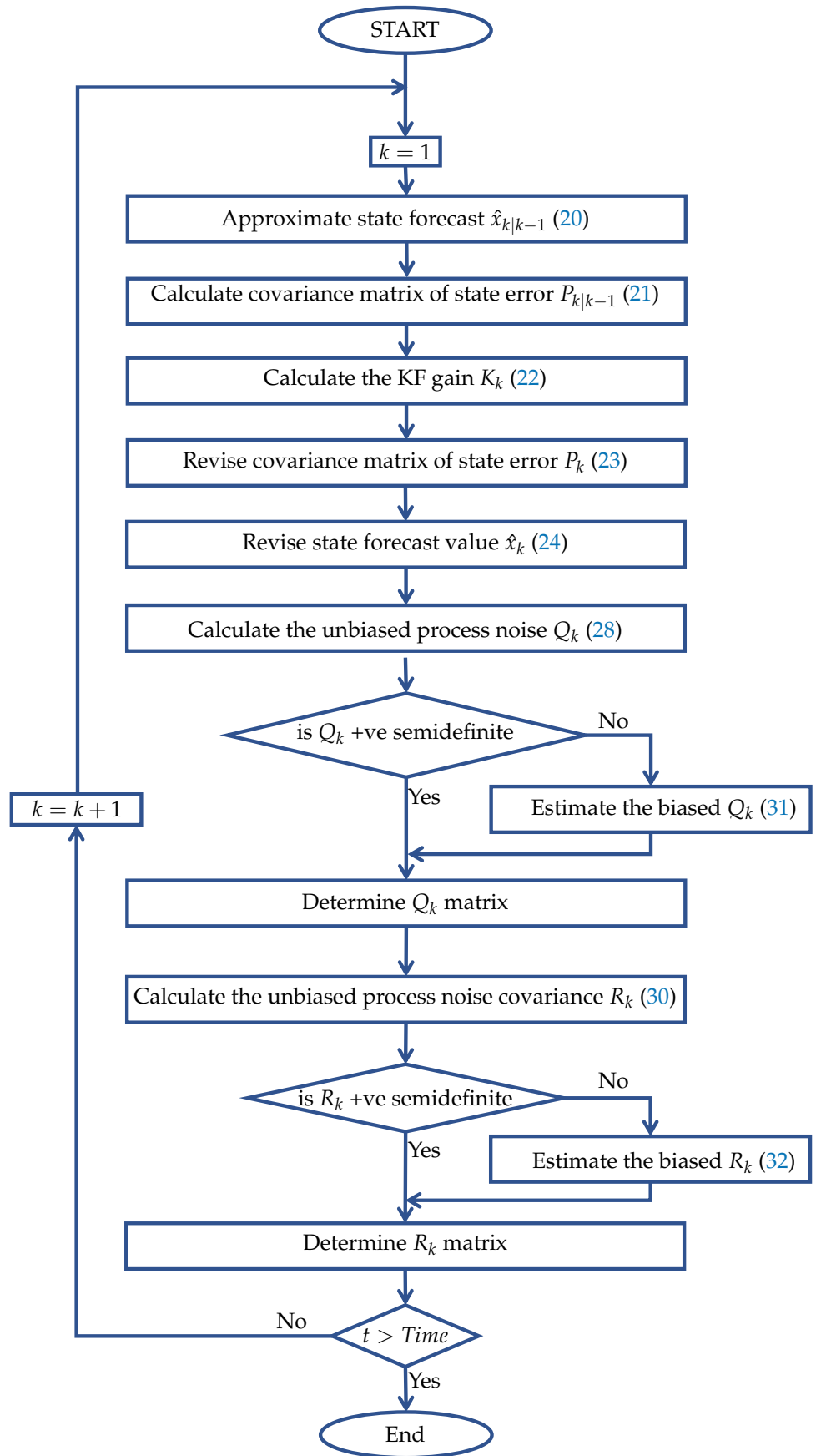


Figure 4. Functional flowchart of parameter identification for AEKF.

Then, by using the initial states of Equation (19) the states are predicted for the future instant by utilizing the following model:

$$\hat{x}_{k|k-1} = \hat{x}_{k-1} + f(\hat{x}_{k-1}, u_{k-1})T + q_{k-1} \quad (20)$$

where the suffix $k - 1$ indicates the parameter value at the instant of t_{k-1} and suffix $k|k - 1$ indicates the predicted parametric value for the instant t_k during the instant of t_{k-1} . T is the sampling period and q is the average value of system process noise.

Further, the approximation of covariance matrix of state error (P) and the Kalman filter gain K are found by utilizing the following dynamics:

$$P_{k|k-1} = \Phi_{k|k-1}P_{k-1}\Phi_{k|k-1}^T + Q_{k-1} \quad (21)$$

$$K_k = P_{k|k-1}H_k^T(H_kP_{k|k-1}H_k^T + R_k)^{-1} \quad (22)$$

where Q_k denotes the system process noise covariance matrix, H_k is the Jacobian matrix, and R_k is the measurement noise covariance matrix. Following that, the covariance matrix and state forecast values are updated for the k^{th} instant as follows:

$$P_k = P_{k|k-1} - K_kH_kP_{k|k-1} \quad (23)$$

$$\hat{x}_k = \hat{x}_{k|k-1} + K_k(z_k - \hat{z}_k) \quad (24)$$

$$\hat{z}_k = H_k\hat{x}_{k|k-1} + r_k \quad (25)$$

where r_k is the average of the measurement system noise; the phasor variables measured in Equation (25) are each PMSG's rating-weighted component results corresponding to the state variables measured at t_k as below:

$$z_k = [i_{md_{eq}}, i_{mq_{eq}}, i_{\omega_{meq}}, v_{dc_{eq}}, i_{gd_{eq}}, i_{gq_{eq}}] \quad (26)$$

For the estimation of the presence of the random noise, a Sage–Husa estimator is used in [71] for the online estimation of the covariance for process noise and measurement noise. Moreover, the estimation method can be performed through biased noise estimation to prevent divergence of the filter but may lead to a larger error in estimation. Hence it should be combined with unbiased noise estimation.

The approximation of the unbiased noise estimation is as follows:

$$q_k = \frac{1}{k} \sum_{j=1}^k [\hat{x}_{j|j} - f(\hat{x}_{j-1|j-1})] \quad (27)$$

$$Q_k = \frac{1}{k} \sum_{j=1}^k \{[\hat{x}_{j|j} - f(\hat{x}_{j-1|j-1}) - q_k][\hat{x}_{j|j} - f(\hat{x}_{j-1|j-1}) - q_k]^T\} \quad (28)$$

$$r_k = \frac{1}{k} \sum_{j=1}^k [z_j - h(\hat{x}_{j|j-1})] \quad (29)$$

$$R_k = \frac{1}{k} \sum_{j=1}^k \{[z_j - h(\hat{x}_{j|j-1}) - r_k][z_j - h(\hat{x}_{j|j-1}) - r_k]^T\} \quad (30)$$

where $t_{j|j}$ is the parameter update of instant t_j .

Then the biased noise estimation is given as

$$Q_k = \frac{1}{k} [(k-1)Q_{k-1} + K_k \varepsilon_k \varepsilon_k^T K_k] \quad (31)$$

$$R_k = \frac{1}{k} [(k-1)R_{k-1} + \varepsilon_k \varepsilon_k^T] \quad (32)$$

where $\varepsilon_k = z_k - \hat{z}_k$.

The algorithm presented in Figure 4 is implemented through iterative operation, and the parameters of PMSG-based WTSs are estimated by utilizing the IEEE-39 bus system. Further, the measurement of variables is achieved through simulation, and the extended state variables x' are identified. The identified parameters are compared under three methods, (i) EKF with randomly occurring noise, (ii) EKF with no random noise, and (iii) AEKF with randomly occurring noise. Further, the comparison of results is carried out under four different cases of (1) sudden change in wind velocity, (2) varying power angle of PMSG, (3) sudden change in system load, and (4) sudden change in the line of the system. From the findings of parameter identification, it has been inferred that the parameters L_f , Ψ_f , and C are highly affected by randomly occurring noise than the parameters L_{md} and L_{mq} in both low and high-disturbance situations. While the identification data of analogous PMSG parameters acquired by AEKF exhibit good resilience, the identification results of different scenarios produced by EKF are inconsistent.

In addition to the above comparative analysis, the authors of [56] have extended the validation procedures to verify the effect of selecting Q and R matrices in the estimation efficacy. The results indicate that the EKF estimation performance is much more prone to the initial values of Q and R matrices. On the other hand, the real-time estimation of matrices in the AEKF method leads to a minimum impact on estimation accuracy. Finally, the precision of the equivalent scheme is substantiated by the simulation of the entire model under AEKF compared with the equivalent model under the capacity-weighted method and particle swarm optimization algorithm. At the same time, EKF gives a solution to the nonlinear estimation problem by linearizing state and/or measurement equations and using the standard Kalman filter descriptions to the available linear estimation problem. The linearization gets to approximation errors which the filter does not consider in the prediction/update process. Therefore, EKF error estimates may perform erroneous estimations of state uncertainties. In addition to this, the authors in [72] have confirmed that the AEKF method cannot give a convergent estimation with adjusted window size.

4.3. Ensemble Kalman Filter-Based Dynamic State Estimation

Furthermore, the 16-variable, complete nonlinear state space model of the grid side MPPT of PMSG-based WTS utilized in the EKF-based dynamic estimation methods discussed in [45,56] has been applied with an ensemble Kalman filter (ENKF) in the article [73]. The ENKF is utilized to propagate the probability distributions of many samples with high accuracy. The state prediction with ENKF utilizes the following dynamics:

ENKF Prediction:

$$\begin{cases} \bar{x}_{k,i} = f(\bar{x}_{k-1,i}, u_{k-1}) + w_{k-1,i} & \text{for } k \geq 1, i = 1, \dots, n \\ \bar{z}_{k,i} = h(\bar{x}_{k-1,i}, u_k) & \text{for } k \geq 1, i = 1, \dots, n \\ \bar{x}_k = \frac{1}{n} \sum_{i=1}^n \bar{x}_{k,i} \\ \bar{z}_k = \frac{1}{n} \sum_{i=1}^n \bar{z}_{k,i} \end{cases} \quad (33)$$

ENKF Correction:

$$\begin{cases} x_{k,i} = \bar{x}_{k,i} + K_k(z_{k,i} - \bar{z}_{k,i}) \\ K_k = \bar{P}_k H_k^T (H_k \bar{P}_k H_k^T + R_k)^{-1} \\ \bar{P}_k H_k^T = \frac{1}{n} \sum_{i=1}^n (\bar{x}_{k,i} - \bar{x}_k)(\bar{z}_{k,i} - \bar{z}_k)^T \\ H_k \bar{P}_k H_k^T = \frac{1}{n} \sum_{i=1}^n (\bar{z}_{k,i} - \bar{z}_k)(\bar{z}_{k,i} - \bar{z}_k)^T \end{cases} \quad (34)$$

where n is the samples representing the distribution, $w_{k-1,i}$ is sample generated in accordance with process noise covariance matrix Q_k , and $x_{k,i}$ is the sample of *posteriori* states. \bar{x}_k , \bar{P}_k , and K_k are, respectively, *priori* mean, *priori* covariance, and ensemble Kalman gain.

z_k and H_k are measurements and Jacobian matrices. Then, the robustness and estimation efficacy is validated by calculating the error indexes under two different cases. Moreover, the Monte-Carlo statistical framework is considered to compare estimated values under EKF, UKF, ENKF, and the actual simulated results. In case-i, the performance analysis is performed with the presence of a large noise and initial values for the states with x_0 . The process and measurement noise's covariance matrices Q_k and R_k are assumed with some random values. Then, in case-ii, the grid's voltage is assumed to be 0 pu for a certain duration of the simulation time. In both cases, ENKF is found to be estimating the present values with better accuracy. Rather, the estimated currents with EKF and UKF methods fluctuate with a magnitude of 0.1 pu. Though we justify the method in [73] with convincing accuracy in estimation, it is noted that the results verification is carried out only on the dq -axes currents of PMSG.

On the other hand, the Kalman filter-based state estimation technique was extended to a sensorless control of a PMSG by considering a single-machine infinite-bus model of the PMSG [74–76]. To increase the estimate accuracy of the system's state variables by eliminating linearization approximations, a derivative-free nonlinear Kalman filter (DFNKF) is introduced in [74–76] to perform sensorless control of the PMSG. In this article, the linearized model is applied to the system using the standard Kalman filter recursion to accomplish the following state estimation. The linearization transformation is based on the differential flatness theory. The suggested methodology gives estimates of the state vector of the PMSG without the necessity for derivatives and Jacobian calculation, in contrast to the Lie algebra-based estimator design method. Therefore, it is claimed that the suggested filtering method reduces the tracking error of the related control loop and produces smooth control signal changes.

4.4. Unscented Kalman Filter-Based Dynamic State Estimation

The Unscented Kalman filter is another augmentation of the Kalman filtering technique that utilizes the unscented transform (UT) to assess the nonlinearity present in the system model [77]. The mean value of a probability distribution with the identical covariance as the states will be treated as the present estimation of the state. Depending on the implementation, different points are selected near the present average value for a full-order UT and reduced-order UT. The EKF techniques discussed earlier utilize the Jacobian matrix to linearize the system model; on the contrary, the UKF technique utilizes the concept of approximating the sigma points [78]. The UKF algorithm begins with the initialization of the state and covariance matrices as follows:

State initialization:

$$\begin{cases} \hat{x}_0 = [\hat{x}_0 \quad 0 \quad 0] \\ P_0 = E[(x_0 - x\hat{x}_0)(x_0 - x\hat{x}_0)^T] = \begin{bmatrix} P_0 & 0 & 0 \\ 0 & Q_k & 0 \\ 0 & 0 & R_k \end{bmatrix} \\ x_{k-1} = [\hat{x}_{k-1} \quad \hat{x}_{k-1} \quad \pm\sqrt{(L+\gamma)P_{k-1}}] \end{cases} \quad (35)$$

where L is the state dimension, $\gamma = \alpha^2[(L+k) - L]$, $\alpha = 1$, and k is taken as zero.

Then, the sigma points of state X_{k-1} are calculated based on (16) as follows,
Sigma points calculation:

$$\begin{cases} \hat{x}_{k|k-1} = \sum_{i=0}^{2L} W_i^m X_{i,k|k-1} \\ \hat{y}_{k|k-1} = \sum_{i=0}^{2L} W_i^c Y_{i,k|k-1, i,k|k-1} \end{cases} \quad (36)$$

where W_i^m and W_i^c are the weighting factors, which can be written as $\frac{1}{2(L+\gamma)}$.

Prediction:

$$\begin{cases} P_{k|k-1} = \sum_{i=0}^{2L} W_i^c (X_{i,k|k-1} - \hat{x}_{k|k-1})(X_{i,k|k-1} - \hat{x}_{k|k-1})^T \\ \hat{y}_{k|k-1} = \sum_{i=0}^{2L} W_i^c Y_{i,k|k-1} \end{cases} \quad (37)$$

Measurement Update:

$$\begin{cases} \bar{P}_{yy} = \sum_{i=0}^{2L} W_i^c (Y_{i,k-1} - \hat{y}_{k|k-1})(Y_{i,k-1} - \hat{y}_{k|k-1})^T \\ \bar{P}_{xy} = \sum_{i=0}^{2L} W_i^c (X_{i,k|k-1} - \hat{x}_{k|k-1})(Y_{i,k-1} - \hat{y}_{k|k-1})^T \\ \hat{x}_k = \hat{x}_{k|k-1} + K_k(y_k - \hat{y}_{k|k-1}) \\ K_k = \bar{P}_{xy} \bar{P}_{yy}^{-1} \\ P_k = P_{k|k-1} + K_k(\bar{P}_{yy})K_k^T \end{cases} \quad (38)$$

where \bar{P}_{yy} and \bar{P}_{xy} are the sigma points of the posterior sigma states $\hat{y}_{k|k-1}$ and $\hat{x}_{k|k-1}\hat{y}_{k|k-1}$.

The above procedure of parameter estimation is being used for the PMSG model given in (5) for state prediction in comparison with the KF and EKF [78]. In the comparative analysis, it is found that the initial error in the estimated states for UKF is much higher due to the improper state initialization. Then, the final steady-state error in UKF reduces near zero and performs better than the KF and EKF techniques. On the other hand, the computational complexity of UKF is found to be higher than the other filtering techniques.

In addition to this, the UKF estimation technique is extensively used to identify the PMSG model with frequency control, swing dynamics, and turbine-governor model with secondary and primary control blocks [79]. From this study, in comparison with EKF, the UKF takes the sigma point samples from the filtering distribution and passes them through the (nonlinear) state and measurement models. The outcome of the weighted set of sigma points gives the revised filtering distribution, which is further estimated as an instant-matched Gaussian distribution. Which gives state estimates that represent the superior estimates over the EKF with high computational complexity. Moreover, the comparison of UKF and EKF in [80] reveals that UKF requires a much higher compilation time than EKF. Additionally, the extended compilation duration of UKF results is due to the sigma points. The accuracy of UKF is found to be higher than EKF, and it does not require Jacobian matrices. In many of the applications, the estimation of Jacobian matrices incurs some difficulty for the control algorithms.

4.5. Cubature Kalman Filter-Based Dynamic State Estimation

In contrast to EKF, CKF does not require the linearization of the nonlinear model or the computation of the Jacobian matrix, which helps address the issue of substandard positioning precision and error divergence brought on by linear truncation. The flexibility of CKF is greater than that of UKF. In a lower-dimensional subspace, CKF cubature points symmetrically appear, and their respective weights are all equal. In the context of this, CKF is considered to be a strong tool for solving the nonlinear estimating issue in the integrated navigation system [81]. The cubature Kalman filter has exhibited a better response for the estimation of synchronous generators in [82]. The generalized procedure for implementing the CKF requires state equations with a set of dynamic and measurement equations, which are given as follows

$$\begin{cases} \dot{x} = f(x(t), u(t)) + w(t) \\ z(t_{k+1}) = h(x(t_{k+1}), u(t_{k+1})) + v(t_{k+1}) \end{cases} \quad (39)$$

where $x(t)$ is the state vector, $u(t)$ is the system input, and $z(t_k)$ is the measurement available at t_k . $w(t)$ and $v(t)$ are the model and measurement noises that are the Gaussian processes with covariance matrices Q and R .

The discrete form of (39) is arrived at by considering a time step Δt as follows:

$$\begin{cases} x_{k+1} = x_k + \Delta t \cdot f(x_k, u_k) + w_{k+1} \\ z_{k+1} = h(x_{k+1}, u_{k+1}) + v_{k+1} \end{cases} \quad (40)$$

Time update:

An estimated state vector of size L , \hat{x}_k , and the covariance matrix corresponding to its estimation error, P_k , are accessible from the previous step at each instant k . These values are used to determine a set of $2L$ cubature points, which are determined as follows:

$$\begin{cases} S_k S_k^T = P_k \\ x_k^i = S_k \xi_i \sqrt{L} + \hat{x}_k \text{ for } i = 1, \dots, 2L \end{cases} \quad (41)$$

where S is the positive definite square matrix root of matrix P , and ξ_i is the i^{th} cubature node. In CKF, the cubature points are least affected by numerical inaccuracy.

The state function f in (40) is evaluated at cubature points for the vectors $x_{k+1|k}^i$. By using this, the a priori estimation is calculated as follows:

$$\begin{cases} \hat{x}_{k+1|k} = \frac{1}{2L} \sum_{i=1}^{2L} x_{k+1|k}^i \\ \hat{P}_{k+1|k} = \frac{1}{2L} \sum_{i=1}^{2L} x_{k+1|k}^i x_{k+1|k}^{iT} - \hat{x}_{k+1|k} \hat{x}_{k+1|k}^T + Q_{k+1} \end{cases} \quad (42)$$

Measurement Update:

The following dynamics are used in the update phase of CKF:

$$\begin{cases} S_{k+1|k} S_{k+1|k}^T = P_{k+1|k} \\ x_{k+1|k}^i = S_{k+1|k} \xi_i \sqrt{L} + \hat{x}_{k+1|k} \text{ for } i = 1, \dots, 2L \\ \gamma_{k+1|k}^i = h(x_{k+1|k}^i, u_k) \text{ for } i = 1, \dots, 2L \\ \hat{z}_{k+1|k}^i = \frac{1}{2L} \sum_{i=1}^{2L} \gamma_{k+1|k}^i \\ \hat{P}_{k+1|k}^z = \frac{1}{2L} \sum_{i=1}^{2L} \gamma_{k+1|k}^i \gamma_{k+1|k}^{iT} - \hat{z}_{k+1|k} \hat{z}_{k+1|k}^T + R_{k+1} \\ \hat{P}_{k+1|k}^{xz} = \frac{1}{2L} \sum_{i=1}^{2L} x_{k+1|k}^i \gamma_{k+1|k}^{iT} - \hat{x}_{k+1|k} \hat{z}_{k+1|k}^T \\ K_{k+1} = P_{k+1|k}^{xz} (P_{k+1|k}^z)^{-1} \end{cases} \quad (43)$$

where $x_{k+1|k}^i$ is the new cubature points, $\hat{z}_{k+1|k}^i$ is the measurement estimation, $\hat{P}_{k+1|k}^z$ is the covariance of measurement estimation, $\hat{P}_{k+1|k}^{xz}$ is the cross-covariance matrix of state and measurements, and K_{k+1} denotes the Kalman gain.

Posteriori prediction:

$$\begin{cases} \hat{x}_{k+1} = \hat{x}_{k+1|k} + K_{k+1} (z_{k+1} - \hat{z}_{k+1}) \\ P_{k+1} = P_{k+1|k} - K_{k+1} \hat{P}_{k+1|k}^z K_{k+1}^T \end{cases} \quad (44)$$

CKF is more suited to problems with increased dimensions, does not involve parameter selection, and has higher numerical stability and estimation accuracy. As a result, it is extensively used in many industrial fields, such as mobile communications, nonlinear parameter estimation, and signal processing in the power system. When designing a cubature Kalman filter, however, the a priori statistical characteristics of the noise should be

precisely determined, along with the EKF algorithm. On the one hand, the a priori statistical characteristics of the noise constrained by testing samples in the practical application are unknown and incorrect. Moreover, when the system is at its actual operating point, a number of unpredictable elements lead the noise's statistical features to become complex and time-varying. Thus, time-varying noise estimation cannot be handled by classic CKF approaches in an adaptive manner. Particularly in the system equations, if there is some uncertainty, unknown noise statistics change with time, and severe disturbances happen in the real world. Then, it is probably going to cause the filtering accuracy to degrade and, even worse.

4.6. Adaptive Cubature Kalman Filter-Based Dynamic State Estimation

An adaptive cubature Kalman filter (ACKF)-based dynamic state estimation technique for the voltage source converter operation was presented in [83]. The most common topology of a grid-connected inverter and control scheme depicted in Figure 1 is used to build a mathematical model of the GSC. Additionally, to facilitate the real-time iterative update of the posterior behavior of the process noise by performing the recursive filtering, the dynamic state estimation is made using the ACKF method, which is an enhancement of the cubature Kalman filtering mixed with the Sage–Husa adaptive filter. As a result, the ACKF is claimed to be more flexible and accurate in its estimations than the CKF. The simulation outcomes demonstrate the viability and precision of the suggested method for grid-side converters. The detailed modeling of grid-side voltage source converter involves the modeling of various components, such as (i) the dc-link as given in (7), (ii) ac side of the converter represented as dq -axes voltages as modeled in (8), (iii) dc-voltage control loop, (iv) dq -axes current control loop, and (v) phase-locked loop (PLL). A typical PI controller has been utilized in the dc-link voltage regulation, dq -axes current control, and PLL, whose dynamics can be referred to in [55,83,84].

The following state space model, which includes the dynamic behavior of the dc-link, dc voltage regulation loop, current control loop, and , can be established with the continuous state function f as follows:

$$\frac{dx}{dt} = f_c(x, u) \quad (45)$$

where x and y are the state vector with dimension n and p -dimensional input vector.

$$\begin{cases} x = [v_{dc} & x_{v_{dc}} & x_{i_{gd}} & i_{gd} & x_{i_{gq}} & i_{gq} & \theta_{PLL} & x_{PLL}]^T \\ y = [i_{dc_{in}} & i_{dc} & v_{dc}^* & u_a & u_b & u_c]^T. \end{cases}$$

where in the state vector x , the various intermediate variables $x_{v_{dc}}$, $x_{i_{gd}}$, $x_{i_{gq}}$, x_{PLL} are the integration result of the PI controller used in dc-link, dq -axes, and PLL controller loop, respectively. In the input vector u , i_{in} is the input current to the dc-link, i_{dc} is the dc-link output current, v_{dc}^* is the dc-link reference voltage, and u_{abc} are the instantaneous grid voltages of phases abc .

Further, the state estimation algorithm requires a set of measurements z through the measurement function h and the sensing system

$$z = [v_{dc} \quad i_{ga} \quad i_{gb} \quad i_{gc} \quad \theta_{PLL}]^T \quad (46)$$

where i_{gabc} are the instantaneous values of grid line currents.

The presumption of a prior behaviors of the process and measurement noise is a well-known shortcoming of Kalman filtering methods in practical systems. Usually, actual data or simulation results are examined to derive the a priori statistics. During the operation, they are taken for granted to remain the same, and they are not updated to reflect the posterior behavior in accordance with the current operational condition and the most recent

data. To solve this issue, recursive filtering is executed with fresh data while the CKF is enhanced by utilizing the adaptive filtering using the Sage–Husa method (39)–(44) for an iterative update of posterior behavior of the process noise. This method is known as ACKF. The continuous state function f_c of the GSC (45) must be discretized due to implications of practical sampling speed. The required modification to the CKF for making it ACKF is explained below.

The measurement noise w_k and the stochastic process v_k are considered as independent, non-stationary Gaussian white noise sequences with the following characteristics:

$$\begin{cases} E(w_k) = q_k, D(w_k) = Q_k \\ E(v_k) = r_k, D(v_k) = R_k \end{cases} \quad (47)$$

where q_k and r_k are the averages of the process and measurement noise w_k and v_k , respectively; Q_k and R_k are the covariance matrices of the w_k and v_k , respectively.

In CKF, it is specifically assumed that the means of q_k and r_k are both zero and that the covariance matrices Q_k and R_k are assumed to be constant. The Sage–Husa adaptive filter, however, updates the states and recursively modifies the Q_k and R_k using the most recent data. Still, the simultaneous correction of Q_k and R_k is unfeasible. Hence, several approaches are used to deal with the noise due to the variations in the error origin and attributes between noise parameters. Additionally, the measurement noise’s statistical properties are typically steady. However, the process noise has discretization errors and model errors connected to the time-step, discretization process, input unreliability, and disturbance. As a result, the process noise is very uncertain and time-variable. Therefore, we assume that the measurement noise’s mean value is zero and its covariance R becomes constant. During the iteration, just the statistical properties of the process noise covariance Q is addressed by the following dynamics,

$$\begin{cases} \hat{q}_{k+1} = (1 - d_k)\hat{q}_k + d_k K_{k+1} r_{k+1} \\ \hat{Q}_{k+1} = (1 - d_k)\hat{Q}_k + d_k (K_{k+1} r_{k+1} r_{k+1}^T K_{k+1}^T + P_{k+1}) - \frac{1}{2L} \sum_{i=1}^{2L} x_{k+1|k}^i x_{k+1|k}^{iT} - \hat{x}_{k+1|k} \hat{x}_{k+1|k}^T \end{cases} \quad (48)$$

where $d_k = (1 - b)/(1 - b^{k+1})$, and b ranges from 0.95–1 [85].

The correction of the posterior statistics of the process noise given in (48) is added to the CKF algorithm given in (39)–(44). Finally, there has been a thorough investigation into the application of dynamic state estimation to GSC from the perspectives of estimation precision and real-time effectuating. The authors have claimed that the ACKF technique is feasible in terms of estimating speed and accuracy, which has the capability to update the posterior behavior of the process noise in real-time and also conduct recursive filtering operations. However, the following drawbacks should be considered,

1. It takes more computation to cope with the correlation estimation compared to the CKFs without the correlation on multiplicative noise.
2. The filtering technique will inevitably grow a little more complicated in order to account for the multiplicative noise component.
3. When the correlation on multiplicative noise is taken into account, the calculation of the suggested filter is likewise increased.
4. The filtering process clearly grows difficult because the correlation coefficient is dynamically estimated.

As a result, the suggested adaptive CKF becomes more sophisticated. The impact on operating efficiency is, however, comparatively minimal due to the current CPU technology’s rising excellent running performance at a reasonable cost [81].

5. Review of State Estimation Techniques for PMSG-Based WTS Fault Diagnosis

The filtering techniques have been widely used in fault diagnosis of WTS applications in many areas, such as blade pitch system and gearbox [86–88]. Primarily, the PMSGs are susceptible to faults that compromise the dependability of the system's functioning, just like most electrical machinery. In PMSG, there are different kinds of faults, among which the stator inter-turn short circuit faults, sensor faults, rotor demagnetization faults, and eccentricity (static, dynamic, and mixed) are not detected by standard protective mechanisms [89]. The fault current flows throughout the machine, especially in the case of PMSG, without significantly affecting the output load current. Consequently, it might result in mechanical and electrical imbalances [90].

The stator inter-turn fault diagnosis of PMSG using the state estimation techniques was analyzed in [91,92]. They used the EKF and UKF state estimation techniques as the model-based fault detection technique. The effectiveness of these two methods is being analyzed based on the response accuracy and convergence speed. The block diagram of the online fault detection mechanism for PMSG is depicted in Figure 5.

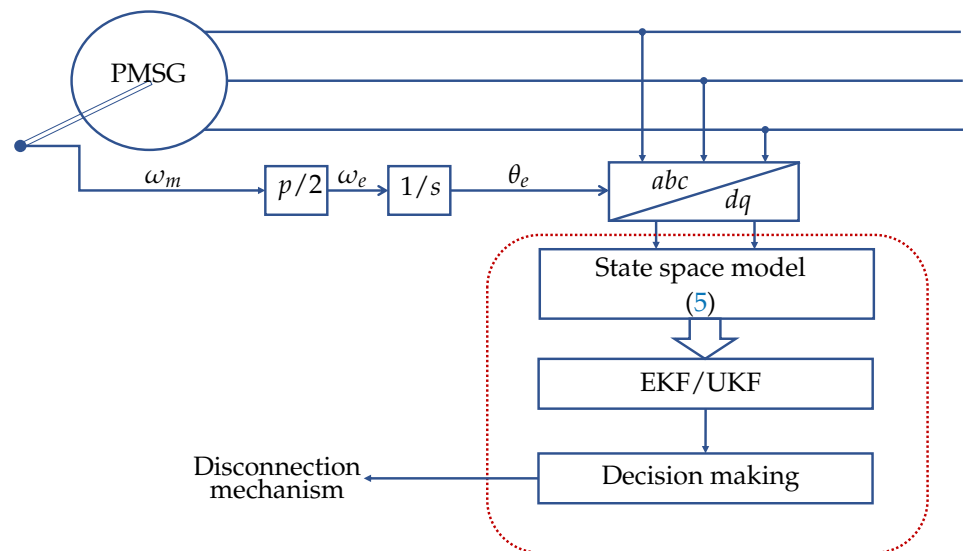


Figure 5. Inter-turn fault detection based on EKF/UKF.

The EKF and UKF parameter estimations are experimentally verified under (i) the noise-free case, (ii) with the presence of measurement noises, and (iii) varying frequency and load. From the obtained results, it has been concluded that the UKF-based diagnosis has better accuracy and fast response.

The PMSG-based WTS needs one position sensor, dc-link voltage sensor, and few voltage and current sensors to achieve good control performance. Any of these sensors failing could cause the system to function improperly or possibly become unstable. As a result, in modern driving systems, sensor fault tolerant control becomes a critical concern [93]. An innovative sensor fault detection and isolation approach based on EKF is proposed in [67]. Then, the EKF-based state estimation technique is experimentally verified for the diagnosis of sensor fault in permanent magnet machines. The EKF is realized by utilizing the time domain machine dynamics given in (5). The state vector is taken as $x = [\Psi_{fd} \ \Psi_{fq} \ \omega_e \ \theta_e]^T$, the input vector is taken as $u = [v_\alpha \ v_\beta]^T$, and the output is taken as $y = [i_a \ i_c]^T$; the detailed procedure of calculating the gradient and measurement matrices can be found in [67]. Additionally, a decision-making unit receives the measured and EKF-estimated angular velocity and phase currents in order to identify the faulty sensor, as shown in Figure 6.

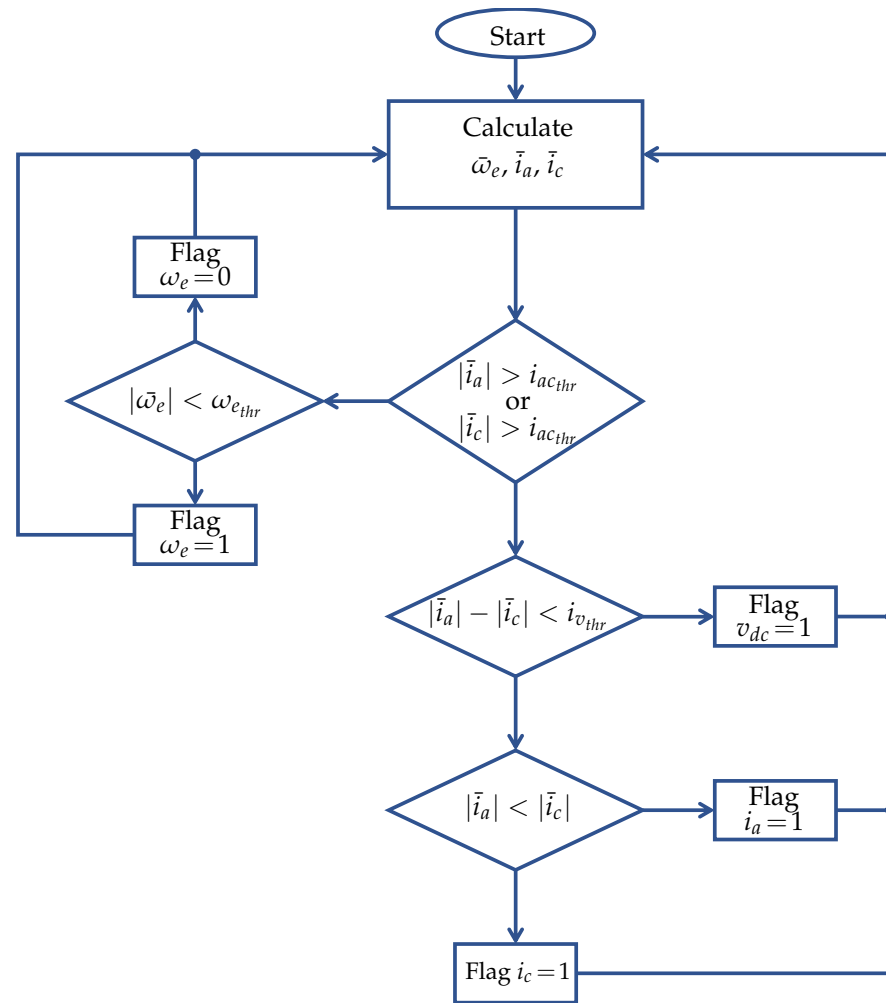


Figure 6. Algorithm to diagnose the sensor faults with EKF.

The dynamics of the variables $\bar{\omega}_e$, \bar{i}_a , and \bar{i}_c are given as follows:

$$\begin{cases} \bar{\omega}_e = \omega_e - \hat{\omega}_e \\ \bar{i}_a = i_a - \hat{i}_a \\ \bar{i}_c = i_c - \hat{i}_c \end{cases} \quad (49)$$

where $\bar{\omega}_e$ is the rotor velocity index, \bar{i}_a denotes the index of a -phase current, and \bar{i}_c denotes the index of c -phase current. The variables denoted with $(\hat{\cdot})$ indicate the estimated variables from EKF. The supremacy of the proposed scheme in sensor fault-tolerant control is confirmed by hardware implementation results, and it is concluded that the response of the algorithm decays at very low speeds and, to a significant extent, the parameter fluctuation has some impact.

6. Observers and Sensorless Control of PMSG-Based WTS

To get rid of the mechanical degradation-prone, low-reliability rotor position, and speed sensing system, the sensorless operation of PMSG is much more prevalent in the industrial control system. The precise online estimation of machine parameters is required to ascertain the machines' position/speed control under sensorless control. Moreover, the efficacy of WTS MPPT operation highly relies on the error-free speed estimation system. Over the past decade, research on this has focused on estimating these important parameters by applying standard filtering techniques. A comparative analysis of speed estimators

with highly noisy measurement signals for Wind Energy Generation Systems was carried out in [94]. A square root-extended Kalman filter (SREKF)-based estimation technique was introduced in [95] for sensorless control of a permanent magnet machine. To perform this, a fixed-point implementation is considered for EKF. The square-root decomposition of the covariance matrices effectively addresses the problem of sensitivity to the round errors in EKF. Moreover, the suitability of many square-root algorithms was compared for this specific application, such as Bierman–Thorton, Carlson–Schmidt–Givens, and Carlson–Schmidt–Householder. With the simulation and experimental results, the Carlson–Schmidt–Givens algorithm can estimate the rotor speed even below 1 Hz. Finally, the SREKF is found to be operating with improved accuracy and robustness.

Then, a detailed discussion is made on the EKF-based estimation technique for online identifications of the magnetic flux of PMSG is made in [96]. A rotor-flux-oriented vector control with model reference adaptive system (MRAS)-based rotor position/speed estimation is used as the baseline control of a permanent magnet machine. The identification problem due to the lower-order state equations has refrained, and the estimated flux value is found to be very minimal.

The conditions under which the estimation of electrical parameters, such as magnetic flux, rotor speed, or other quantities, are only sometimes sufficiently investigated in many of the estimation methods applicable to the PMSG system. To deal with this issue, an AC drive observability analysis with states having robust speed and position approximation is made in [97]. In this article, the authors have proposed a nonlinear system state observability theory to evaluate a general scheme for ac-drive observability investigation.

Further, a fault-tolerant controller with state observers for a permanent magnet machine is discussed in [98]. The scheme uses an EKF estimation and back-electromotive-force adaptive observer as virtual sensors to build a fault-tolerant control design. On the other hand, a nonlinear Luenberger-like observer-based control for the PMSG wind turbine is evaluated to estimate the mechanical variables, which only uses information on the electrical parameter. The estimates are then used to formulate a strategy for MPPT operation without a mechanical sensor [99]. Then, an MPPT operation of PMSG-based WTS using a linear observer and adaptive fractional order PID controller is discussed in [100]. The combined effect of stochastic wind speed change, parameter uncertainties, generator nonlinearities, and unaccounted dynamics are taken into a perturbation; then the real-time estimation is carried out by a linear extended-state observer known as a high-gain state and perturbation observer. Moreover, the comparative results for rotor speed estimation reveal that the Kalman filtering-based estimation has a better response time with minimum ripples. On the other hand, the accuracy is lower than the phase-locked loop-based estimation [94].

7. State Estimation Techniques for Wind Turbine Pitch and Yaw Control

7.1. Sliding Mode Observer-Based State Estimation for Pitch Actuator

State estimation is an algorithmic procedure of getting state variables from the network measurements. The state estimation method for wind turbine pitch systems under sliding mode observer (SMO) is the efficient method to provide satisfactory results; the entire structure is given in Figure 7. For this, the single-pitch system is presented in [101] and expressed as follows:

$$\begin{cases} \dot{x}_1 = x_2 \\ \dot{x}_2 = -\omega_n^2 x_1 - 2\zeta\omega_n x_2 + \omega_n^2 u \\ y = x_1 \end{cases} \quad (50)$$

where $[x_1 \ x_2]^T = [\beta \ \dot{\beta}]^T$ denotes the states of the system, and $u - \beta_r$ is the input control variable. β , $\dot{\beta}$, ω_n , and ζ are the pitch angle, angular velocity, natural frequency, and damping factor, respectively. Additionally, the above-mentioned dynamic model can be remodeled under convex combination methods derived in the following form:

$$\begin{cases} \dot{x}_1 = x_2 \\ \dot{x}_2 = G_0(x) - B_0u + F(x)f \\ y = x_1 \end{cases} \tag{51}$$

where $G_0(x) = -\omega_{no}^2x_1 - 2\zeta_o\omega_{no}x_2$, $B_0 = \omega_{no}^2$, and $F(x) = (\omega_{no}^2 - \omega_{nf}^2)(x_1 - u) + 2(\zeta_o\omega_{no} - \zeta_f\omega_{nf})x_2$.

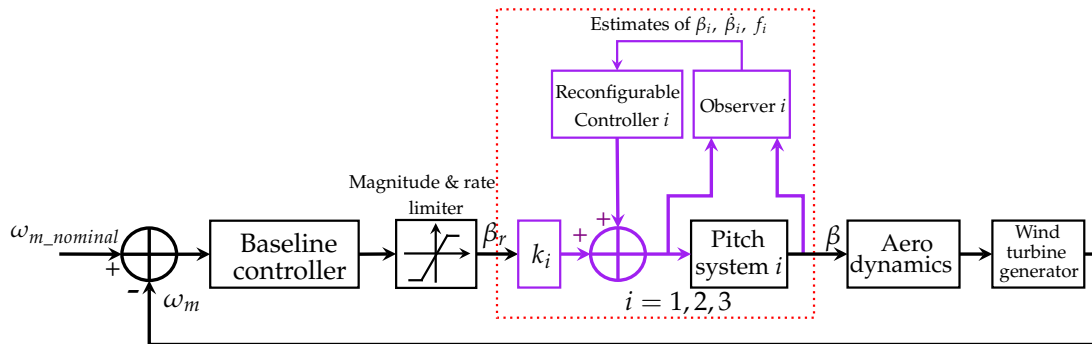


Figure 7. Schematic diagram of pitch control with SMO.

The sliding mode observer (SMO) is modified in this method to estimate system states. Additionally, the SMO incorporates the adaptive technique, resulting in prior knowledge of the estimation error bounds not being necessary. Then, the SMO is given as

$$\begin{cases} \dot{\hat{x}}_1 = \hat{x}_2 + v_1 \\ \dot{\hat{x}}_2 = G_0(\hat{x}) - B_0u + F(\hat{x})\hat{f} + v_2 \\ \dot{\hat{f}} = \eta_f \text{sign}(e_f) \end{cases} \tag{52}$$

where $\hat{x} = [\hat{x}_1 \ \hat{x}_2]^T$ are the state estimates. \hat{f} is denoted by the estimation of fault. Following this, the estimation errors of states is $e_{x1} = x_1 - \hat{x}_1$, $e_{x2} = x_2 - \hat{x}_2$ and fault is $e_f = f - \hat{f}$, respectively. Then, the switching function of SMO is given by

$$v_1 = \eta_{v1} \text{sign}(e_{x1}), v_2 = \eta_{v2} \text{sign}(e_{x2} - \dot{\hat{x}}_2) \tag{53}$$

where η_{v1}, η_{v2} , and η_f represent design parameters.

Furthermore, most of the nonlinear observer approaches have limitations since they require precise knowledge of the model’s structure and parameters. In [101,102], the adoption of sliding modes can overcome these limitations. From (52), the modified SMO was derived to estimate the states of the pitch actuator with fault conditions.

7.2. Estimation of States for Yaw Control of Wind Turbine

The yaw controller controls the yaw system by rotating the nacelle to face the wind direction, aiming to minimize the yaw angle Θ_{yaw} error, which can maximize the power extraction. However, the yaw control system depends on the wind direction information. Thus, light detection and ranging (LIDAR) have allowed the acquirement of continuous previewed wind knowledge, including wind speed and wind direction [103]. In the aspect of yaw control design, the authors in [104] have proposed an adaptive model predictive approach based on a yaw control method for a wind turbine system. The stochastic model predictive yaw control was presented in [105] using the predicted wind direction to estimate the future and best yaw rate for the large-scale wind turbine system. The authors in [106] presented an active yaw control technique for the HAWT system without requiring the wind direction measurement for a small-scale system. On the other side, the state estimation method has been widely used in the wind turbine’s control, as explained earlier; thus,

estimating the wind turbine yaw system in the literature is limited. However, the authors in [107] used the Kalman filter estimation method for forecasting wind direction to assist the wind turbine yaw control. Based on the target system type, the Kalman filter algorithm is classified into linear and extended KF. The authors in [108] have used the linear KF algorithm based on the linear ARIMA model to estimate the wind information's for the yaw control system. The step-by-step procedure is as follows: (1) system modeling, (2) measurement update, and (3) time update filter gain. The detailed design is given in the following step-by-step procedure.

1. Modeling: The initial step is to represent the system dynamic model in a general format as

$$\begin{cases} x(t+1) = Ax(t) + w(t+1) \\ y(t+1) = Cx(t) + v(t+1) \end{cases} \quad (54)$$

where $x(t+1)$ and $y(t+1)$ are regarded as the state and measurement, respectively; $w(t+1)$ and $v(t+1)$ give the state and measurement noises.

2. Measurement updating: The following dynamics can be used as the measurement update

$$\begin{cases} x(t+1) = x\left(\frac{t+1}{t}\right) + K(t+1)(y(t+1) - Cx\left(\frac{t+1}{t}\right)) \\ K(t+1) = P\left(\frac{t+1}{t}\right)C^T(CP\left(\frac{t+1}{t}\right)C^T + R(t+1))^{-1} \\ P(t+1) = (I - K(t+1)C)P\left(\frac{t+1}{t}\right) \end{cases} \quad (55)$$

where $K(t+1)$ is the Kalman gain, $P(t+1)$ denotes state estimation error covariance, and $R(t+1)$ gives the measurement noise covariance.

3. Time update filter gain: The time update is fulfilled by

$$\begin{cases} x\left(\frac{t+2}{t+1}\right) = Ax(t+1) \\ P\left(\frac{t+2}{t+1}\right) = AP(t+1)A^T + Q(t+1) \end{cases} \quad (56)$$

where $Q(t+1)$ is the state noise covariance. Therefore, all the model parameters of KF-based wind direction estimator are given in detail, refer to [108]. Hence, the proposed KF-estimator offered better results in wind prediction. In the end, the power extraction from the wind turbine using MPC-based yaw control has improved with a KF-based wind direction estimator.

8. Conclusions

In this article, various state estimation techniques applicable to the precise modeling, control, and monitoring of interfacing systems and energy conversion systems of WTSs have been reviewed through various literature studies. The nonlinear modeling of PMSG-based WTS with a full rated converter has been performed to analyze and evaluate the various state estimation techniques. The various components and control systems exhibiting a higher degree of complications, uncertainty, and highly nonlinear control problems involved in PMSG-based WTS have been considered for estimation. The state estimation techniques have been identified to reduce the effect of noises and present all hidden variables, which is found to be beneficial, especially in control procedures, such as low-voltage ride-through operation, MPP tracking, inter-turn fault detection, sensorless control, and active power regulation. Analysis and summary of popular state estimation techniques, such as EKF, AEKF, UKF, CKF, and ACKF, which deal with the real-time information of operating variables through filters and observers, have been analyzed for PMSG-based WTSs. Additionally, it has been identified that concise research still needs to be improved for estimating states in pitch control and yaw control of WTS. Finally, the future direction of research may consider modeling the entire system structure of WTS, including pitch, yaw dynamics, and the application of state estimation techniques to such a model.

Author Contributions: G.M., R.P.A., R.V. and K.P.: Conceptualization, Methodology, Writing—Original draft and validation. Y.H.J., S.R.L. and D.S.: Supervision, Method Validation, Writing—Review and Editing. All authors have read and agreed to the published version of the manuscript.

Funding: This work was supported in part by the Basic Science Research Program under Grant NRF-2016R1A6A1A03013567 and by the framework of International Cooperation Program under Grant NRF-2022K2A9A2A06045121 through the National Research Foundation of Korea (NRF) funded by the Ministry of Education, and National natural science foundation of China under Grant 62211540397.

Conflicts of Interest: The authors declare no conflict of interest.

Nomenclature

The following notations are used in this manuscript:

P	wind turbine aerodynamic power
ρ	air density
V_w	wind speed
C_p	power co-efficient
λ	tip speed ratio
ω_m	rotor speed
R	radius of turbine blade
β	pitch angle
J_{eq}	moment of inertia
T_{ad}	aerodynamic torque
T_{em}	electromagnetic torque
B	viscous friction coefficient
v_{mdq}, i_{mdq}	dq -axes voltage and current of machine
R_s	stator resistance
L_{mdq}	stator inductances in dq frame
Ψ_f	magnetic flux
v_{dc}	dc-link voltage
C	dc-link capacitance
P_e, P_g	stator and grid electric powers
v_{fdq}, i_{gdq}	dq -axes voltage and current of filter
R_f	filter resistance
L_{gdq}	grid inductances in dq frame
ω_f	grid voltage angular frequency
Q_g	grid reactive power
$\{\}_{k+1}$	next state of a parameter
$\{\}_k$	present state of a parameter
$\{\}_{k-1}$	previous state of a parameter
A, B, C	state, input, and output matrices of a system
T_s	sampling period
P, Q, R	state covariance, process noise, measurement noise
F	Jacobians of the state functions

References

1. Jones, D. *Global Electricity Review 2021*; Ember: London, UK, 2021.
2. Palanimuthu, K.; Mayilsamy, G.; Basheer, A.A.; Lee, S.R.; Song, D.; Joo, Y.H. A Review of Recent Aerodynamic Power Extraction Challenges in Coordinated Pitch, Yaw, and Torque Control of Large-Scale Wind Turbine Systems. *Energies* **2022**, *15*, 8161.
3. Soares-Ramos, E.P.; de Oliveira-Assis, L.; Sarrias-Mena, R.; Fernández-Ramírez, L.M. Current status and future trends of offshore wind power in Europe. *Energy* **2020**, *202*, 117787.
4. Darwish, A.S.; Al-Dabbagh, R. Wind energy state of the art: Present and future technology advancements. *Renew. Energy Environ. Sustain.* **2020**, *5*, 7.
5. GWEC. *Global Offshore Wind Report 2020*; GWEC: Brussels, Belgium, 2020; Volume 19, pp. 10–12.
6. López-Queija, J.; Robles, E.; Jugo, J.; Alonso-Quesada, S. Review of control technologies for floating offshore wind turbines. *Renew. Sustain. Energy Rev.* **2022**, *167*, 112787.

7. Haces-Fernandez, F.; Cruz-Mendoza, M.; Li, H. Onshore Wind Farm Development: Technologies and Layouts. *Energies* **2022**, *15*, 2381.
8. Nejad, A.R.; Keller, J.; Guo, Y.; Sheng, S.; Polinder, H.; Watson, S.; Dong, J.; Qin, Z.; Ebrahimi, A.; Schelenz, R.; et al. Wind turbine drivetrains: State-of-the-art technologies and future development trends. *Wind Energy Sci.* **2022**, *7*, 387–411.
9. Heng, T.Y.; Ding, T.J.; Chang, C.C.W.; Ping, T.J.; Yian, H.C.; Dahari, M. Permanent Magnet Synchronous Generator design optimization for wind energy conversion system: A review. *Energy Rep.* **2022**, *8*, 277–282.
10. Ma, J.; Xu, H.; Zhang, M.; Cheng, P. Stability analysis of sub/super synchronous oscillation in direct-drive wind farm considering the energy interaction between PMSGs. *IET Renew. Power Gener.* **2022**, *16*, 478–496.
11. Shu, T.; Song, D.; Joo, Y.H. Non-centralised coordinated optimisation for maximising offshore wind farm power via a sparse communication architecture. *Appl. Energy* **2022**, *324*, 119705.
12. Chen, Y.; Joo, Y.H.; Song, D. Multi-Objective Optimisation for Large-Scale Offshore Wind Farm Based on Decoupled Groups Operation. *Energies* **2022**, *15*, 2336.
13. Padinharu, D.K.K.; Li, G.J.; Zhu, Z.Q.; Clark, R.; Thomas, A.; Azar, Z.; Duke, A. Permanent magnet vernier machines for direct-drive offshore wind power: Benefits and Challenges. *IEEE Access* **2022**, *10*, 20652–20668.
14. Kim, B. Design method of a direct-drive permanent magnet vernier generator for a wind turbine system. *IEEE Trans. Ind. Appl.* **2019**, *55*, 4665–4675.
15. Kim, H.W.; Kang, S.G.; Jung, S.Y.; Yeo, H.K. Design and Analysis of Permanent-Magnet Vernier Machine for Direct-Driven Wind Power Generator Considering Pole-Slot Combinations. *J. Electr. Eng. Technol.* **2022**, *18*, 319–327.
16. Ghaheri, A.; Afjei, E.; Torkaman, H. Design optimization of a novel linear transverse flux switching permanent magnet generator for direct drive wave energy conversion. *Renew. Energy* **2022**, *198*, 851–860.
17. Padinharu, D.K.K.; Li, G.J.; Zhu, Z.Q.; Clark, R.; Thomas, A.S.; Azar, Z. System-level investigation of multi-MW direct-drive wind power PM vernier generators. *IEEE Access* **2020**, *8*, 191433–191446.
18. Tlali, P.M.; Wang, R.J.; Gerber, S.; Botha, C.D.; Kamper, M.J. Design and performance comparison of vernier and conventional PM synchronous wind generators. *IEEE Trans. Ind. Appl.* **2020**, *56*, 2570–2579.
19. Palanimuthu, K.; Mayilsamy, G.; Lee, S.R.; Jung, S.Y.; Joo, Y.H. Comparative analysis of maximum power extraction and control methods between PMSG and PMVG-based wind turbine systems. *Int. J. Electr. Power Energy Syst.* **2022**, *143*, 108475. <https://doi.org/10.1016/j.ijepes.2022.108475>.
20. Joo, Y.H.; Antonysamy, R.; Ramasamy, T.; Lee, S.R. Stable maximum power extraction and DC link voltage regulation for PMVG-based WECS. *IEEE Trans. Ind. Electron.* **2022**, *70*, 498–508.
21. Antonysamy, R.P.; Lee, S.R.; Jung, S.Y.; Joo, Y.H. Performance Enhancement Using Robust Sliding Mode Approach-Based Current Control for PMVG-WECS. *IEEE Trans. Ind. Electron.* **2022**, 1–10. <https://doi.org/10.1109/TIE.2022.3220859>
22. Venkateswaran, R.; Yesudhas, A.A.; Lee, S.R.; Joo, Y.H. Integral sliding mode control for extracting stable output power and regulating DC-link voltage in PMVG-based wind turbine system. *Int. J. Electr. Power Energy Syst.* **2023**, *144*, 108482.
23. Primadianto, A.; Lu, C.N. A review on distribution system state estimation. *IEEE Trans. Power Syst.* **2016**, *32*, 3875–3883.
24. Abur, A.; Exposito, A.G. *Power System State Estimation: Theory and Implementation*; CRC Press: Boca Raton, FL, USA, 2004.
25. NERC. *Power Plant Dynamic Model Verification Using PMUs*; NERC Reliability: Atlanta, GA, USA, 2016.
26. Berg, J.C.; Miller, K. *Sensor Selection for Wind Turbine State Estimation*; Technical Report; Sandia National Lab. (SNL-NM): Albuquerque, NM, USA, 2008.
27. He, X.; Wang, Z.; Liu, Y.; Zhou, D.H. Least-squares fault detection and diagnosis for networked sensing systems using a direct state estimation approach. *IEEE Trans. Ind. Inform.* **2013**, *9*, 1670–1679.
28. Abhinav, S.; Pal, B.C. *Dynamic Estimation and Control of Power Systems*; Academic Press: Cambridge, MA, USA, 2018.
29. Rostami, M.; Lotfifard, S. Distributed dynamic state estimation of power systems. *IEEE Trans. Ind. Inform.* **2017**, *14*, 3395–3404.
30. Huang, Z.; Schneider, K.; Nieplocha, J. Feasibility studies of applying Kalman filter techniques to power system dynamic state estimation. In Proceedings of the 2007 International Power Engineering Conference (IPEC 2007), Singapore, 3–6 December 2007; pp. 376–382.
31. Karimipour, H.; Dinavahi, V. Extended Kalman filter-based parallel dynamic state estimation. *IEEE Trans. Smart Grid* **2015**, *6*, 1539–1549.
32. Jafarzadeh, S.; Lascu, C.; Fadali, M.S. State estimation of induction motor drives using the unscented Kalman filter. *IEEE Trans. Ind. Electron.* **2011**, *59*, 4207–4216.
33. González-Cagigal, M.; Rosendo-Macías, J.A.; Gómez-Expósito, A. Parameter estimation of wind turbines with PMSM using cubature Kalman filters. *IEEE Trans. Power Syst.* **2019**, *35*, 1796–1804.
34. Zhao, J.; Mili, L. A theoretical framework of robust H-infinity unscented Kalman filter and its application to power system dynamic state estimation. *IEEE Trans. Signal Process.* **2019**, *67*, 2734–2746.
35. Qi, J.; Sun, K.; Wang, J.; Liu, H. Dynamic state estimation for multi-machine power system by unscented Kalman filter with enhanced numerical stability. *IEEE Trans. Smart Grid* **2016**, *9*, 1184–1196.
36. Zhou, N.; Meng, D.; Lu, S. Estimation of the dynamic states of synchronous machines using an extended particle filter. *IEEE Trans. Power Syst.* **2013**, *28*, 4152–4161.
37. Cui, Y.; Kavasseri, R. A particle filter for dynamic state estimation in multi-machine systems with detailed models. *IEEE Trans. Power Syst.* **2015**, *30*, 3377–3385.

38. Emami, K.; Fernando, T.; Iu, H.H.C.; Trinh, H.; Wong, K.P. Particle filter approach to dynamic state estimation of generators in power systems. *IEEE Trans. Power Syst.* **2014**, *30*, 2665–2675.
39. Zhang, T.; Zhang, W.; Yuan, P. Distributed dynamic state estimation in active distribution system based on particle filter. In Proceedings of the 2018 IEEE Innovative Smart Grid Technologies-Asia (ISGT Asia), Singapore, 22–25 May 2018; pp. 664–668.
40. El-Sharafy, M.Z.; Saxena, S.; Farag, H.E. Optimal design of islanded microgrids considering distributed dynamic state estimation. *IEEE Trans. Ind. Inform.* **2020**, *17*, 1592–1603.
41. Ritter, B.; Schild, A.; Feldt, M.; Konigorski, U. The design of nonlinear observers for wind turbine dynamic state and parameter estimation. *J. Phys. Conf. Ser.* **2016**, *753*, 052029.
42. Noor-A-Rahim, M.; MO Khyam, X.L.; Pesch, D. Sensor fusion and state estimation of IoT enabled wind energy conversion system. *Sensors* **2019**, *19*, 1566.
43. Mateljak, P.; Petrovic, V.; Baotic, M. Dual kalman estimation of wind turbine states and parameters. In Proceedings of the International Conference on Process Control, Tatranska Lomnica, Slovakia, 14–17 June 2011; pp. 85–91.
44. Miranda-Blanco, B.N.; Díaz-Dorado, E.; Carrillo, C.; Cidrás, J. State estimation for wind farms including the wind turbine generator models. *Renew. Energy* **2014**, *71*, 453–465.
45. Shahriari, S.A.A.; Raoofat, M.; Dehghani, M.; Mohammadi, M.; Saad, M. Dynamic state estimation of a permanent magnet synchronous generator-based wind turbine. *IET Renew. Power Gener.* **2016**, *10*, 1278–1286.
46. Yu, S.; Fernando, T.; Emami, K.; Iu, H.H.C. Dynamic state estimation based control strategy for DFIG wind turbine connected to complex power systems. *IEEE Trans. Power Syst.* **2016**, *32*, 1272–1281.
47. Yu, S.; Emami, K.; Fernando, T.; Iu, H.H.; Wong, K.P. State estimation of doubly fed induction generator wind turbine in complex power systems. *IEEE Trans. Power Syst.* **2016**, *31*, 4935–4944.
48. Prajapat, G.P.; Bhui, P.; Senroy, N.; Kar, I.N. Modelling and estimation of gear train backlash present in wind turbine driven DFIG system. *IET Gener. Transm. Distrib.* **2018**, *12*, 3527–3535.
49. Bourlis, D.; Bleijs, J. A wind speed estimation method using adaptive Kalman filtering for a variable speed stall regulated wind turbine. In Proceedings of the 2010 IEEE 11th International Conference on Probabilistic Methods Applied to Power Systems, Singapore, 14–17 June 2010; pp. 89–94.
50. Sudev, P.; Anita, J.; Sudheesh, P. Nonlinear state estimation of wind turbine. In Proceedings of the 2017 International Conference on Advances in Computing, Communications and Informatics (ICACCI), Udupi, India, 13–16 September 2017; pp. 354–358.
51. Song, D.; Yang, J.; Cai, Z.; Dong, M.; Su, M.; Wang, Y. Wind estimation with a non-standard extended Kalman filter and its application on maximum power extraction for variable speed wind turbines. *Appl. Energy* **2017**, *190*, 670–685.
52. Shahriari, S.A.A.; Mohammadi, M.; Raoofat, M. A new method based on state-estimation technique to enhance low-voltage ride-through capability of doubly-fed induction generator wind turbines. *Int. J. Electr. Power Energy Syst.* **2018**, *95*, 118–127.
53. Ibrahim, R.A.; Zakzouk, N.E. A PMSG Wind Energy System Featuring Low-Voltage Ride-through via Mode-Shift Control. *Appl. Sci.* **2022**, *12*, 964.
54. Kumar, A.; Ghosh, S.; Das, S.; Singh, A.K.; Singh, N.K. ANFIS-Based Control for Low-Voltage Ride-Through Enhancement of PMSG Tidal Turbine. In Proceedings of the 2022 IEEE Students Conference on Engineering and Systems (SCES), Prayagraj, India, 1–3 July 2022; pp. 1–6.
55. Palanimuthu, K.; Mayilsamy, G.; Lee, S.R.; Jung, S.Y.; Joo, Y.H. Fault Ride-through for PMVG-based Wind Turbine System Using Coordinated Active and Reactive Power Control Strategy. *IEEE Trans. Ind. Electron.* **2022**, 1–11. <https://doi.org/10.1109/TIE.2022.3194638>.
56. Shahriari, S.A.A.; Mohammadi, M.; Raoofat, M. Enhancement of low-voltage ride-through capability of permanent magnet synchronous generator wind turbine by applying state-estimation technique. *COMPEL Int. J. Comput. Math. Electr. Electron. Eng.* **2020**, *39*, 363–377.
57. Yin, X.; Jiang, Z.; Pan, L. Recurrent neural network based adaptive integral sliding mode power maximization control for wind power systems. *Renew. Energy* **2020**, *145*, 1149–1157.
58. Nasiri, M.; Milimonfared, J.; Fathi, S. A review of low-voltage ride-through enhancement methods for permanent magnet synchronous generator based wind turbines. *Renew. Sustain. Energy Rev.* **2015**, *47*, 399–415.
59. Venkateswaran, R.; Natesan, B.; Lee, S.R.; Joo, Y.H. Maximum Power Extraction for PMVG-based WECS Using Q-Learning MPPT Algorithm with Finite-time Control Scheme. *IEEE Trans. Sustain. Energy* **2022**, *14*, 516–524.
60. Joo, Y. Integral sliding mode control for increasing maximum power extraction efficiency of variable-speed wind energy system. *Int. J. Electr. Power Energy Syst.* **2022**, *139*, 107958.
61. Mayilsamy, G.; Natesan, B.; Joo, Y.H.; Lee, S.R. Fast Terminal Synergetic Control of PMVG-Based Wind Energy Conversion System for Enhancing the Power Extraction Efficiency. *Energies* **2022**, *15*, 2774.
62. Yesudhas, A.A.; Joo, Y.H.; Lee, S.R. Reference Model Adaptive Control Scheme on PMVG-Based WECS for MPPT under a Real Wind Speed. *Energies* **2022**, *15*, 3091.
63. Kuppasamy, S.; Joo, Y.H. Stabilization Criteria for T-S Fuzzy Systems With Multiplicative Sampled-Data Control Gain Uncertainties. *IEEE Trans. Fuzzy Syst.* **2021**, *30*, 4082–4092.
64. Kuppasamy, S.; Joo, Y.H. Observer-Based Non-PDC Control Design for PMSG-Based Wind Energy Conversion Systems. *IEEE Trans. Syst. Man Cybern. Syst.* **2022**. 1–8. <https://doi.org/10.1109/TSMC.2022.3217568>.

65. Ramasamy, T.; Abdul Basheer, A.; Tak, M.H.; Joo, Y.H.; Lee, S.R. An Effective DC-Link Voltage Control Strategy for Grid-Connected PMVG-Based Wind Energy Conversion System. *Energies* **2022**, *15*, 2931.
66. Kalman, R.E. A new approach to linear filtering and prediction problems. *Trans. ASME J. Basic Eng.* **1960**, *82*, 35–45.
67. Foo, G.H.B.; Zhang, X.; Vilathgamuwa, D.M. A sensor fault detection and isolation method in interior permanent-magnet synchronous motor drives based on an extended Kalman filter. *IEEE Trans. Ind. Electron.* **2013**, *60*, 3485–3495.
68. Huang, H.; Mao, C.; Lu, J.; Wang, D. Small-signal modelling and analysis of wind turbine with direct drive permanent magnet synchronous generator connected to power grid. *IET Renew. Power Gener.* **2012**, *6*, 48–58.
69. Xie, D.; Xu, Z.; Yang, L.; Østergaard, J.; Xue, Y.; Wong, K.P. A comprehensive LVRT control strategy for DFIG wind turbines with enhanced reactive power support. *IEEE Trans. Power Syst.* **2013**, *28*, 3302–3310.
70. Wang, T.; Huang, S.; Gao, M.; Wang, Z. Adaptive extended Kalman filter based dynamic equivalent method of PMSG wind farm cluster. *IEEE Trans. Ind. Appl.* **2021**, *57*, 2908–2917.
71. Narasimhappa, M.; Mahindrakar, A.D.; Guizilini, V.C.; Terra, M.H.; Sabat, S.L. MEMS-based IMU drift minimization: Sage Husa adaptive robust Kalman filtering. *IEEE Sens. J.* **2019**, *20*, 250–260.
72. Zhang, S.; Zhang, C.; Jiang, S.; Zhang, X. A comparative study of different adaptive extended/unscented Kalman filters for lithium-ion battery state-of-charge estimation. *Energy* **2022**, *246*, 123423.
73. Afrasiabi, S.; Afrasiabi, M.; Rastegar, M.; Mohammadi, M.; Parang, B.; Ferdowsi, F. Ensemble kalman filter based dynamic state estimation of PMSG-based wind turbine. In Proceedings of the 2019 IEEE Texas Power and Energy Conference (TPEC), College Station, TX, USA, 7–8 February 2019; pp. 1–4.
74. Rigatos, G.; Siano, P.; Zervos, N. PMSG sensorless control with the Derivative-free nonlinear Kalman Filter for Distributed Generation units. *IFAC Proc. Vol.* **2013**, *46*, 9–14. <https://doi.org/10.3182/20130703-3-FR-4038.00009>.
75. Rigatos, G.; Siano, P.; Zervos, N. Derivative-free nonlinear Kalman filtering for PMSG sensorless control. In *Interdisciplinary Mechatronics*; Wiley: Hoboken, NJ, USA, 2013; pp. 277–311.
76. Rigatos, G.; Siano, P.; Zervos, N. PMSG sensorless control with the use of the derivative-free nonlinear Kalman filter. In Proceedings of the 2013 International Conference on Clean Electrical Power (ICCEP), Alghero, Italy, 11–13 June 2013; pp. 673–678.
77. Turner, R.; Rasmussen, C.E. Model based learning of sigma points in unscented Kalman filtering. *Neurocomputing* **2012**, *80*, 47–53. <https://doi.org/10.1016/j.neucom.2011.07.029>.
78. Gliga, L.I.; Chafouk, H.; Popescu, D.; Lupu, C. Comparison of State Estimators for a Permanent Magnet Synchronous Generator. In Proceedings of the 2018 22nd International Conference on System Theory, Control and Computing (ICSTCC), Sinaia, Romania, 10–12 October 2018; pp. 474–479.
79. Aghamolki, H.G.; Miao, Z.; Fan, L.; Jiang, W.; Manjure, D. Identification of synchronous generator model with frequency control using unscented Kalman filter. *Electr. Power Syst. Res.* **2015**, *126*, 45–55. <https://doi.org/10.1016/j.epsr.2015.04.016>.
80. LaViola, J.J. A comparison of unscented and extended Kalman filtering for estimating quaternion motion. In Proceedings of the Proceedings of the 2003 American Control Conference, Denver, CO, USA, 4–6 June 2003; Volume 3, pp. 2435–2440.
81. Liu, M.; Lai, J.; Li, Z.; Liu, J. An adaptive cubature Kalman filter algorithm for inertial and land-based navigation system. *Aerosp. Sci. Technol.* **2016**, *51*, 52–60.
82. Pillai, D.G.; Vivek, A.; Srikanth, V. Non-linear state estimation of PMSM using derivative-free and square-root Cubature Kalman Filter. In Proceedings of the 2017 International Conference on Intelligent Computing, Instrumentation and Control Technologies (ICICT), Kerala, India, 6–7 July 2017; pp. 126–131.
83. Zhang, J.; Bi, T.; Liu, H. Dynamic state estimation of a grid-connected converter of a renewable generation system using adaptive cubature Kalman filtering. *Int. J. Electr. Power Energy Syst.* **2022**, *143*, 108470.
84. Wu, B.; Lang, Y.; Zargari, N.; Kouro, S. *Power Conversion and Control of Wind Energy Systems*; John Wiley & Sons: Hoboken, NJ, USA, 2011.
85. Zhao, J.; Zheng, Z.; Wang, S.; Huang, R.; Bi, T.; Mili, L.; Huang, Z. Correlation-Aided Robust Decentralized Dynamic State Estimation of Power Systems With Unknown Control Inputs. *IEEE Trans. Power Syst.* **2020**, *35*, 2443–2451. <https://doi.org/10.1109/TPWRS.2019.2953256>.
86. Cho, S.; Choi, M.; Gao, Z.; Moan, T. Fault detection and diagnosis of a blade pitch system in a floating wind turbine based on Kalman filters and artificial neural networks. *Renew. Energy* **2021**, *169*, 1–13.
87. Zhipeng Feng.; Qin, S.; Liang, M. Time–frequency analysis based on Vold-Kalman filter and higher order energy separation for fault diagnosis of wind turbine planetary gearbox under nonstationary conditions. *Renew. Energy* **2016**, *85*, 45–56. <https://doi.org/10.1016/j.renene.2015.06.041>.
88. Omneya Attallah.; Ibrahim, R.A.; Zakzouk, N.E. CAD system for inter-turn fault diagnosis of offshore wind turbines via multi-CNNs & feature selection. *Renew. Energy* **2022**. <https://doi.org/10.1016/j.renene.2022.12.064>.
89. Gliga, L.I.; Chafouk, H.; Popescu, D.; Lupu, C. Diagnosis of a permanent magnet synchronous generator using the extended Kalman filter and the fast Fourier transform. In Proceedings of the 2018 7th International Conference on Systems and Control (ICSC), Valencia, Spain, 24–26 October 2018; pp. 65–70.
90. Otava, L.; Buchta, L. Implementation and verification of the PMSM stator interturn short fault detection algorithm. In Proceedings of the 2017 19th European Conference on Power Electronics and Applications (EPE'17 ECCE Europe), Warsaw, Poland, 11–14 September 2017; pp. P.1–P.10. <https://doi.org/10.23919/EPE17ECCEurope.2017.8099080>.

91. El Sayed, W.; Abd El Geliel, M.; Lotfy, A. Fault diagnosis of PMSG stator inter-turn fault using extended Kalman filter and unscented Kalman filter. *Energies* **2020**, *13*, 2972.
92. El Sayed, W.; Aboelhassan, A.; Madi, A.; Hebala, A.; Galea, M. Comparative Analysis Between Unscented and Extended Kalman Filters for PMSG Inter-Turn Fault Detection. In Proceedings of the 2021 IEEE Workshop on Electrical Machines Design, Control and Diagnosis (WEMDCD), Modena, Italy, 8–9 April 2021; pp. 243–248.
93. Zheng, C.; Chen, Z.; Huang, D. Fault diagnosis of voltage sensor and current sensor for lithium-ion battery pack using hybrid system modeling and unscented particle filter. *Energy* **2020**, *191*, 116504.
94. Carranza, O.; Figueres, E.; Garcerá, G.a.; Gonzalez, L. Comparative study of speed estimators with highly noisy measurement signals for Wind Energy Generation Systems. *Appl. Energy* **2011**, *88*, 805–813.
95. Smidl, V.; Peroutka, Z. Advantages of square-root extended Kalman filter for sensorless control of AC drives. *IEEE Trans. Ind. Electron.* **2011**, *59*, 4189–4196.
96. Shi, Y.; Sun, K.; Huang, L.; Li, Y. Online identification of permanent magnet flux based on extended Kalman filter for IPMSM drive with position sensorless control. *IEEE Trans. Ind. Electron.* **2011**, *59*, 4169–4178.
97. Vaclavek, P.; Blaha, P.; Herman, I. AC drive observability analysis. *IEEE Trans. Ind. Electron.* **2012**, *60*, 3047–3059.
98. Akrad, A.; Hilaiet, M.; Diallo, D. Design of a fault-tolerant controller based on observers for a PMSM drive. *IEEE Trans. Ind. Electron.* **2011**, *58*, 1416–1427.
99. Fantino, R.; Solsona, J.; Busada, C. Nonlinear observer-based control for PMSG wind turbine. *Energy* **2016**, *113*, 248–257. <https://doi.org/10.1016/j.energy.2016.07.039>.
100. Yang, B.; Yu, T.; Shu, H.; Han, Y.; Cao, P.; Jiang, L. Adaptive fractional-order PID control of PMSG-based wind energy conversion system for MPPT using linear observers. *Int. Trans. Electr. Energy Syst.* **2019**, *29*, e2697.
101. Lan, J.; Patton, R.J.; Zhu, X. Fault-tolerant wind turbine pitch control using adaptive sliding mode estimation. *Renew. Energy* **2018**, *116*, 219–231.
102. Gao, R.; Gao, Z. Pitch control for wind turbine systems using optimization, estimation and compensation. *Renew. Energy* **2016**, *91*, 501–515.
103. Scholbrock, A.; Fleming, P.; Wright, A.; Slinger, C.; Medley, J.; Harris, M. *Field Test Results from Lidar Measured Yaw Control for Improved Yaw Alignment with the NREL Controls Advanced Research Turbine*; Technical Report; National Renewable Energy Lab. (NREL): Golden, CO, USA, 2014.
104. Song, D.; Chang, Q.; Zheng, S.; Yang, S.; Yang, J.; Joo, Y.H. Adaptive model predictive control for yaw system of variable-speed wind turbines. *J. Mod. Power Syst. Clean Energy* **2020**, *9*, 219–224.
105. Song, D.; Li, Z.; Wang, L.; Jin, F.; Huang, C.; Xia, E.; Rizk-Allah, R.M.; Yang, J.; Su, M.; Joo, Y.H. Energy capture efficiency enhancement of wind turbines via stochastic model predictive yaw control based on intelligent scenarios generation. *Appl. Energy* **2022**, *312*, 118773.
106. Karakasis, N.; Mesemanolis, A.; Nalmpantis, T.; Mademlis, C. Active yaw control in a horizontal axis wind system without requiring wind direction measurement. *IET Renew. Power Gener.* **2016**, *10*, 1441–1449.
107. Song, D.; Fan, X.; Yang, J.; Liu, A.; Chen, S.; Joo, Y.H. Power extraction efficiency optimization of horizontal-axis wind turbines through optimizing control parameters of yaw control systems using an intelligent method. *Appl. Energy* **2018**, *224*, 267–279.
108. Song, D.; Yang, J.; Liu, Y.; Su, M.; Liu, A.; Joo, Y.H. Wind direction prediction for yaw control of wind turbines. *Int. J. Control Autom. Syst.* **2017**, *15*, 1720–1728.

Disclaimer/Publisher’s Note: The statements, opinions and data contained in all publications are solely those of the individual author(s) and contributor(s) and not of MDPI and/or the editor(s). MDPI and/or the editor(s) disclaim responsibility for any injury to people or property resulting from any ideas, methods, instructions or products referred to in the content.